STEM CELLS

Intestinal Paneth cell differentiation relies on asymmetric regulation of Wnt signaling by Daam1/2

Gabriele Colozza[1]†, Heetak Lee[1,2]†, Alessandra Merenda[3]†, Szu-Hsien Sam Wu[1], Andrea Català-Bordes[1], Tomasz W. Radaszkiewicz[4], Ingrid Jordens[5], Ji-Hyun Lee[1,2], Aileen-Diane Bamford[1,6], Fiona Farnhammer[1,7], Teck Yew Low[8], Madelon M. Maurice[5], Vítězslav Bryja[4,9], Jihoon Kim[1,10]*, Bon-Kyoung Koo[1,2,11]*

The mammalian intestine is one of the most rapidly self-renewing tissues, driven by stem cells residing at the crypt bottom. Paneth cells form a major element of the niche microenvironment providing various growth factors to orchestrate intestinal stem cell homeostasis, such as Wnt3. Different Wnt ligands can selectively activate β-catenin–dependent (canonical) or –independent (noncanonical) signaling. Here, we report that the Dishevelled-associated activator of morphogenesis 1 (Daam1) and its paralogue Daam2 asymmetrically regulate canonical and noncanonical Wnt (Wnt/PCP) signaling. Daam1/2 interacts with the Wnt inhibitor RNF43, and Daam1/2 double knockout stimulates canonical Wnt signaling by preventing RNF43-dependent degradation of the Wnt receptor, Frizzled (Fzd). Single-cell RNA sequencing analysis revealed that Paneth cell differentiation is impaired by Daam1/2 depletion because of defective Wnt/PCP signaling. Together, we identified Daam1/2 as an unexpected hub molecule coordinating both canonical and noncanonical Wnt, which is fundamental for specifying an adequate number of Paneth cells.

INTRODUCTION

The intestinal epithelium provides both a large surface for nutrient uptake as well as a physical barrier against harmful agents such as pathogens, and during homeostasis, new cells are rapidly generated to maintain their functionality (*1*, *2*). It is organized in a villus-crypt structure consisting of numerous cell types, including intestinal stem cells (ISCs) and Paneth cells (PCs) at the crypt bottom. Previous studies have shown that multiple signaling pathways are involved in the homeostatic turnover and differentiation of the intestinal epithelium, with Wnt and Notch signaling playing a key role in ISC maintenance and differentiation (*1*, *3*). The potency of Wnt signaling depends mainly on the cell surface levels of its receptor Fzd, which in turn is controlled by RNF43 and ZNRF3 (RZ), transmembrane E3 ligases that ubiquitinate Fzd and promote its degradation through the endo-lysosomal system, thus tightly controlling Wnt signals (*4*–*6*). RZ are, in turn, regulated negatively by the R-spondin (Rspo) ligand-Lgr4/5 receptor complex (*5*, *7*, *8*) and positively by phosphorylation of their cytoplasmic tail (*9*) as well as by the enzyme USP42 which stabilizes RZ at the plasma membrane (*10*, *11*). In the intestinal epithelium, PCs are the main source of Wnt and Notch ligands (*12*, *13*). Notch signaling controls cell fate determination of the absorptive and secretory lineages, while canonical Wnt signaling regulates ISC maintenance and proliferation (*1*). However, it is still unclear how noncanonical Wnt signaling influences intestinal epithelial homeostasis and differentiation and in which way the noncanonical Wnt signaling is coordinated with canonical Wnt signaling. Here, we demonstrate that Dishevelled-associated activator of morphogenesis 1 (Daam1) and its paralogue Daam2, members of the diaphanous-related formin (DRF) family of Rho guanosine triphosphatase (GTPase) effectors (*14*), function as hub molecules for optimal canonical versus noncanonical Wnt signaling, to maintain appropriate numbers of ISCs and PCs in the intestinal crypt.

RESULTS

Identification of potential RNF43 interactors

To identify potential functional regulators of RNF43, we performed mass spectrometry (MS) analysis using RNF43 as bait, followed by a CRISPR-Cas9 genetic screening (Fig. 1, A to C). From the MS analysis, we captured a number of potential interactors, listed in table S1. To narrow down the list of potential candidates, the following selection criteria were adopted: (i) particular attention was paid to those MS hits showing the greatest number of peptides; (ii) candidates with known expression in the mouse intestine or relevant function were included. For this reason, genes already known to be implicated in processes like ubiquitination, membrane trafficking, the WNT pathway, and endocytosis were of particular interest, as they are all relevant to RNF43 function; (iii) lastly, one additional parameter considered in the selection process was the number of paralogues each gene had. For instance, genes with many paralogues expressed in the intestine were excluded, given the difficulty of obtaining

[1]Institute of Molecular Biotechnology of the Austrian Academy of Sciences (IMBA), Vienna BioCenter (VBC), 1030 Vienna, Austria. [2]Center for Genome Engineering, Institute for Basic Science, 55, Expo-ro, Yuseong-gu, Daejeon 34126, Republic of Korea. [3]HUB Organoids, Utrecht, Netherlands. [4]Department of Experimental Biology, Faculty of Science, Masaryk University, Brno, Czech Republic. [5]Oncode Institute and Centre for Molecular Medicine, University Medical Centre Utrecht, Utrecht, Netherlands. [6]Department of Biosystems Science and Engineering, ETH Zurich, Mattenstrasse 26, 4058 Basel, Switzerland. [7]Division of Metabolism and Division of Oncology, University Children's Hospital Zurich and Children's Research Center, University of Zurich, 8032 Zurich, Switzerland. [8]UKM Medical Molecular Biology Institute (UMBI), University Kebangsaan Malaysia (UKM), Jalan Yaacob Latiff, Bandar Tun Razak, 56000 Kuala Lumpur, Malaysia. [9]Department of Cytokinetics, Institute of Biophysics, Academy of Sciences of the Czech Republic, Brno, Czech Republic. [10]Department of Medical and Biological Sciences, The Catholic University of Korea, Bucheon, Republic of Korea. [11]Department of Life Sciences, Pohang University of Science and Technology (POSTECH), Pohang, Republic of Korea.
*Corresponding author. Email: jhkim@catholic.ac.kr (J.K.); koobk@ibs.re.kr (B.-K.K.)
†These authors contributed equally to this work.

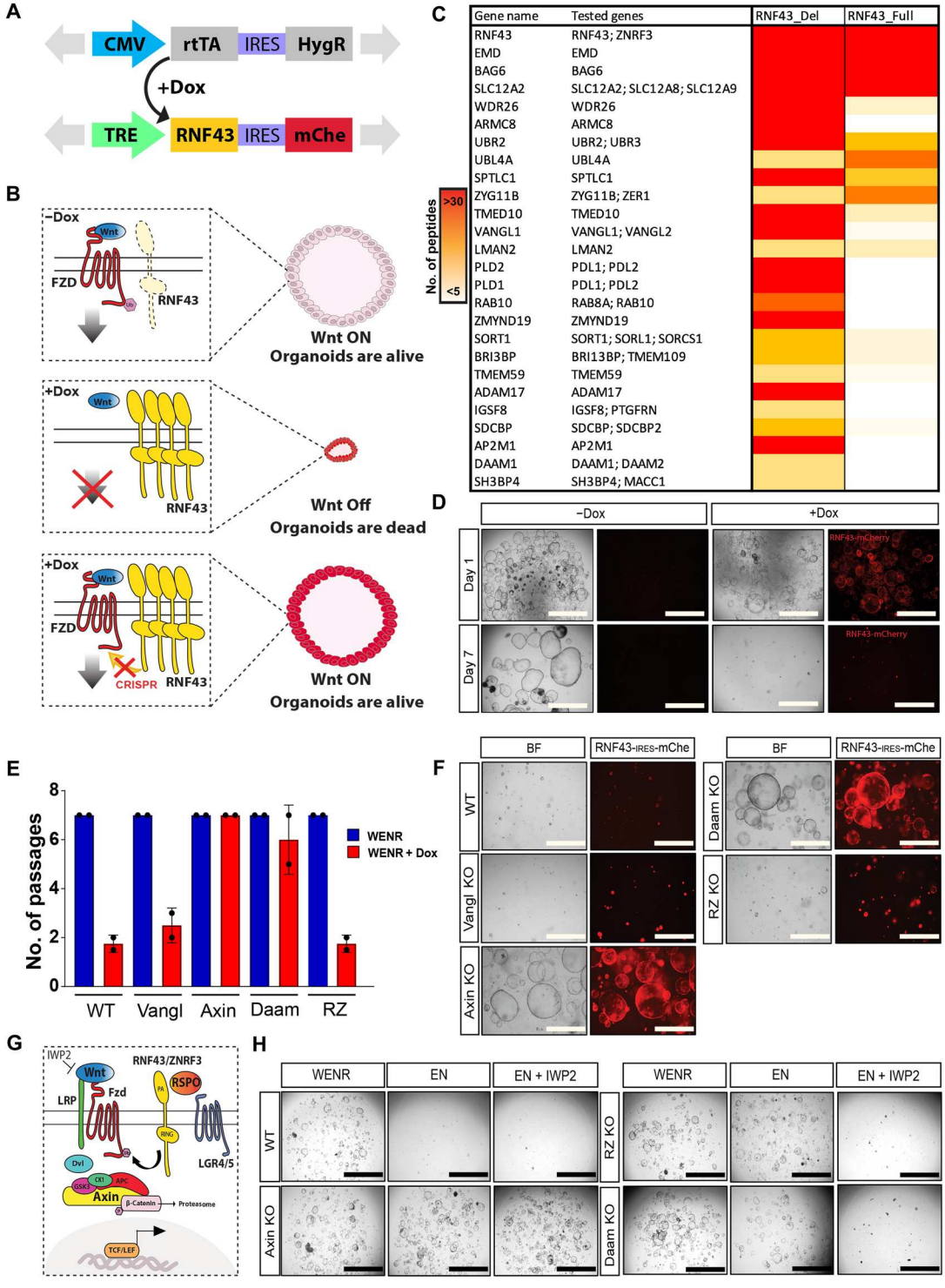

Fig. 1. Functional CRISPR screening of RNF43-interacting proteins. (**A**) Schematic of the DNA constructs used to generate small intestinal organoids expressing doxycycline-inducible *RNF43-IRES-mCherry*. mCherry is used as a proxy for RNF43 expression. (**B**) Schematic showing the CRISPR-based screening of RNF43-expressing organoids. Doxycyclin addition turns on RNF43 expression and organoids die unless downstream components necessary for RNF43 activity are eliminated via CRISPR-Cas9 knockout (KO). (**C**) List of RNF43-interacting proteins identified via mass spectrometry. The abundance of each protein is represented as the number of peptides detected, according to the color scale on the left. Pull-down results from full-length (RNF43_Full) and truncated RNF43 (RNF43_Del) are shown. See Material and Methods for details. (**D**) Organoid assay showing robust RNF43 expression upon doxycycline treatment. Note that, at day 7, all organoids expressing RNF43 (here visualized through mCherry fluorescence) are dead. (**E**) Bar plot quantification of organoid survival after indicated passages. Only Axin and Daam CRISPR-KO organoids grow in the presence of RNF43 overexpression. (**F**) Survival assay of wild-type (WT) and indicated CRISPR KO mutant organoids after RNF43 induction. (**G**) Schematic illustrating the growth factor withdrawal assay used in (H), to determine RNF43 interactor epistasis in the Wnt pathway. (**H**) Growth factor withdrawal assay on WT and indicated CRISPR mutant organoids. All scale bars represent 1000 μm. CMV, cytomegalovirus; IRES, internal ribosomal entry site. BF, brightfield; TCF/LEF, T-cell factor/lymphoid enhancer factor; WENR, Wnt EGF Noggin R-spondin1-containing medium.

simultaneous knockout (KO). In light of the above considerations, not only were the top-ranked hits chosen for further analysis but also those that seemed promising based on their function, irrespective of a low MS score. Thus, by combining all the MS data and considering the abovementioned criteria, a list of 25 genes was drawn up (Fig. 1C).

To functionally test the role of these candidates in RNF43 regulation, we performed a small-scale CRISPR-Cas9 KO screen on mouse small intestinal organoids grown in a standard medium containing Wnt, EGF, Noggin, and R-spondin1 (WENR) (Fig. 1, A to F). Guide RNAs (gRNAs) were designed to knock out paralogue genes as well as to prevent genetic compensation caused by functional redundancy (Fig. 1C) (*15*, *16*). For this purpose, we first

established a mouse small intestinal organoid line expressing *RNF43-IRES-mCherry* (Dox-RNF43 SI organoid) under the control of a doxycycline responsive promoter (Fig. 1, A and B). As expected, in the presence of doxycycline, these organoids rapidly died as a consequence of Wnt blockade by overexpressed RNF43 (Fig. 1D). However, genetic depletion of factors required for RNF43-dependent inhibition of Wnt activity could prevent organoid death by maintaining high levels of canonical Wnt signaling, similar to the KO of other negative regulators of Wnt/β-catenin, such as Axin1/2 (Fig. 1, B, E, and F). Using this screening platform, we identified Daam1 and Daam2 as functional interactors of RNF43 (Fig. 1F). Depletion of Daam1/2 (D1/2 DKO) in Dox-RNF43 organoids could rescue organoid survival as efficiently as Axin1/2 KO (Axin DKO), despite the presence of RNF43 overexpression (Fig. 1F). To test whether Daam1/2 is downstream of the RZ axis (Lgr4/5-Rspo-RZ), we used withdrawal assays for either R-spondin1 (EN medium) or both Wnt and Rspo (EN + the Wnt inhibitor IWP2) (Fig. 1G). As expected, CRISPR-generated Axin DKO organoids survived in both conditions, whereas RZ DKO organoids did not survive without Wnt (Fig. 1H and fig. S1, A and B). In contrast to wild-type (WT) organoids, D1/2 DKO organoids did survive in Rspo deficient medium (EN), but they also died in the Wnt- and Rspo-deficient condition (EN + IWP2) (Fig. 1H and fig. S1B), similar to RZ DKO organoids. These findings suggest that unlike Axin and Apc, which are components of the destruction complex downstream of Wnt and Fzd, Daam1/2 acts at the level of or downstream of the RZ axis, disruption of which renders organoids independent of Rspo but still dependent on Wnt stimulation for optimal canonical Wnt signaling.

In addition to Daam1/2, a few other candidates from the MS hit list emerged as interesting molecules to study in the context of RNF43 activity and, even more broadly, Wnt pathway regulation. For example, KO of Ubl4a, Sec16a, and Slc12a2, together with their paralogues, resulted in organoids viable for more than five passages in doxycycline-supplemented medium, similar to Axin1/2 KO organoids (fig. S1C). In contrast to Daam, none of these genes has ever been associated with the Wnt pathway before. Another interesting hit from our list was Vangl, also a known component of the Wnt/PCP pathway. However, Vangl KO organoids failed to survive under doxycycline-dependent induction of RNF43 (Fig. 1E and fig. S1C) probably because Vangl represents a target of RNF43, rather than a cofactor, as previously demonstrated (*17*). Thus, we focused on Daam1/2 for further characterization due to its known role in noncanonical Wnt signaling (*18*, *19*) and the organoid phenotype described here.

Daam1/2 is essential for RNF43-mediated Fzd endocytosis

Next, we sought to understand how Daam1/2 regulates canonical Wnt signaling in cooperation with RNF43. RNF43, as well as its paralogue ZNRF3, is a well-known E3 ubiquitin ligase that targets Fzd for ubiquitination-mediated endo-lysosomal degradation (*4*, *5*). Hence, we decided to monitor cell surface levels of Fzd in the absence or presence of Daam1/2. To this aim, we knocked out *DAAM1/2* in human embryonic kidney (HEK) 293T cells (D1/2 DKO HEK293T cells) via CRISPR-Cas9 (fig. S2, A and B) and performed receptor internalization assays using a SNAP-tagged Fzd5 construct (Fig. 2A) (*4*). In WT HEK293T cells, SNAP-Fzd5 was rapidly internalized and decreased from the plasma membrane when coexpressed with RNF43. In contrast, D1/2 DKO HEK293T cells maintained higher levels of cell surface Fzd5 (Fig. 2A and fig. S2C). We also assessed the endogenous levels of cell surface Fzd receptors by flow cytometry analysis using a pan-Fzd antibody (*20*). Even in the presence of RNF43, D1/2 DKO HEK293T cells showed increased surface levels of Fzd compared to WT cells, where Fzd levels were down-regulated upon RNF43 overexpression (Fig. 2B). To further corroborate the difference in Fzd internalization between WT and D1/2 KO cells, we used a HibiT/nano-luciferase cell surface detection assay, which allows the quantitation of cell surface–exposed proteins through a two-component complementation luciferase system (Fig. 2C) (*21*–*23*). In the presence of RNF43, only a small fraction of N-terminally HibiT-tagged Fzd5 could be detected by membrane-impermeable LgBiT protein on the surface of WT cells (Fig. 2D). In contrast, much higher levels of Fzd5 were still detected on the plasma membrane of D1/2 DKO HEK293T cells even after cotransfecting RNF43, suggesting a reduction in RNF43-dependent Fzd endocytosis (Fig. 2D). An increase in plasma membrane Fzd5 was also obtained with triple KO of Dishevelled1/2/3 (Dvl TKO) (Fig. 2D), coherently with the known role of Dvl as an essential regulator of Fzd ubiquitination and degradation by RNF43 (*24*). In addition to Fzd, using a cell surface protein biotinylation assay, we found that surface levels of the Wnt co-receptor Lrp6 were also retained in the D1/2 DKO HEK293T cells in the presence of RNF43 (Fig. 3A, lane 5).

To precisely understand the role of Daam1/2 in RNF43-mediated Fzd endocytosis, we investigated RNF43-Daam1/2 interactions and Fzd ubiquitination. First, immunoprecipitation (IP) assay using overexpressed full-length (F.L.) tagged Daam1 and RNF43 showed that RNF43 could efficiently pull-down Myc-tagged Daam1 (Fig. 3B), corroborating our MS data (Fig. 1C). Then, to identify which domain of Daam1 is required for RNF43 interaction, we overexpressed F.L. Daam1, previously described N-term and C-term truncated constructs (*18*), as well as a Daam1 mutant lacking the C-terminal Dvl-interacting diaphanous autoregulatory domain (DAD) (*19*), together with RNF43 in HEK293T cells (Fig. 3C). We were able to precipitate RNF43 together with F.L., N-term, and ΔDAD mutant Daam1 but not with the Dvl-binding C-term Daam1 (Fig. 3D and fig. S3A), indicating that the Daam1 N-terminal domain is necessary and sufficient for its interaction with RNF43 and that binding to Dvl is not required. Accordingly, we found that RNF43 could pull down similar levels of Myc-tagged Daam1 in both WT and Dvl TKO HEK293T cells (fig. S3B). Notably, overexpression of the N-terminal domain, but not the C-terminal domain, could also rescue RNF43-mediated clearance of Lrp6 from the plasma membrane in D1/2 DKO cells (Fig. 3A, lanes 7 and 8). Only a partial effect was observed with F.L. Daam1 (Fig. 3A, lane 6), in line with previous studies reporting that Daam proteins, like other formins, stay in a closed, auto-inhibited conformation (*14*, *18*, *19*).

Next, we checked the effect of D1/2 DKO on RNF43-mediated Fzd interaction, ubiquitination, and degradation. In the absence of Daam1/2 proteins, V5-tagged Fzd5 could still interact with RNF43, as assessed by IP from D1/2 DKO HEK293T cells (fig. S3C), indicating that Daam1/2 does not mediate RNF43 binding to Fzd. On the other hand, Dvl proteins are known to mediate the interaction between Fzd and RNF43 and are required for Fzd degradation (*24*). Thus, we compared Fzd degradation in D1/2 DKO and Dvl TKO HEK293T cells. In the presence of RNF43, Fzd5 was strongly down-regulated in WT HEK293T cells (Fig. 3E, lane 2). Fzd

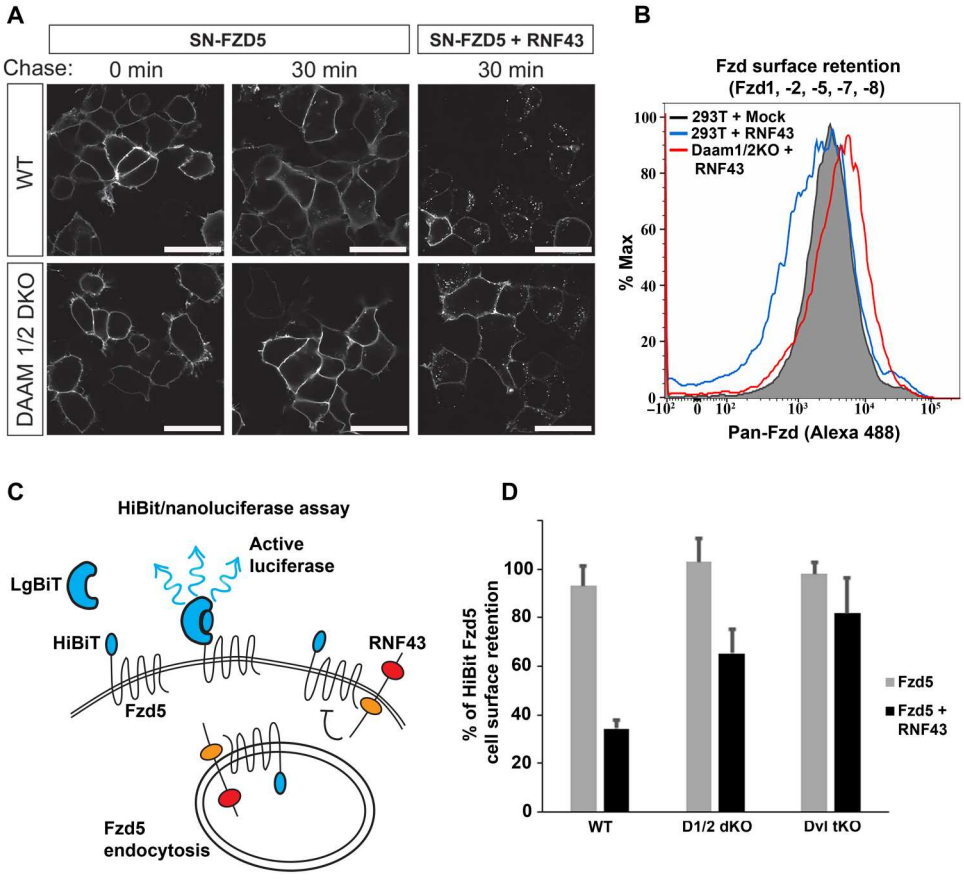

Fig. 2. Daam is required for RNF43-dependent Frizzled endocytosis. (**A**) Subcellular localization of SNAP-Fzd5 in WT or Daam1/2 DKO HEK293T cells cotransfected with control empty vector or RNF43. Surface SNAP-Fzd5 was labeled with SNAP-surface Alexa 549 for 15 min and chased for 30 min. Scale bars, 20 μm. (**B**) Fluorescence-activated cell sorting (FACS) analysis of plasma membrane levels of Fzd receptors in WT and D1/2 DKO HEK293T cells, with or without RNF43 overexpression. (**C**) Schematic of Nano-Glo/HiBiT assay. The N terminus of Fzd5 contains a HibiT tag, to which LgBiT binds, restoring nano-luciferase activity. In the presence of RNF43, less HibiT-Fzd5 is exposed on the plasma membrane, preventing the reconstitution of luciferase activity. (**D**) Nano-Glo–based quantification of cell surface Fzd5. Levels are expressed as percentages of relative light unit fractions. Data from three independent biological experiments.

down-regulation specifically required RNF43 E3 ligase activity, as an RNF43 mutant, lacking the RING catalytic domain, could not induce Fzd degradation (Fig. 3E, lane 3). In D1/2 DKO HEK293T cells, the levels of Fzd5 were reduced but not completely suppressed (Fig. 3E, lanes 4 and 5). The same was observed in the Dvl TKO HEK293T cells (Fig. 3E, lanes 6 and 7), as expected since Dvl bridges the interaction between RNF43 and Fzd (*24*). This indicates that Daam1/2, like Dvl, is necessary for the RNF43-mediated degradation of Fzd.

However, differences were observed between D1/2 DKO HEK293T and Dvl TKO HEK293T in the levels of Fzd ubiquitination: in Dvl TKO cells, Fzd ubiquitination was clearly reduced (Fig. 3F, lane 9), confirming previous observations (*24*). In contrast, D1/2 DKO showed elevated levels of Fzd ubiquitination, even when compared to that of WT HEK293T cells (Fig. 3F, lanes 7 and 8), suggesting that Fzd ubiquitination is still intact in D1/2 DKO HEK293T cells. We speculate that Daam1/2 is necessary for the internalization and subsequent vesicle sorting of ubiquitinated Fzd receptors, whereas Dvl is important for RNF43-Fzd interaction and ubiquitination of Fzd. Together, we propose the following stepwise mechanism of ubiquitination-mediated Fzd endo-lysosomal degradation: First, Dvl promotes the interaction between RNF43 and Fzd, leading to Fzd ubiquitination, after which Daam1/2 promotes the internalization and subsequent sorting of ubiquitinated Fzd. From this model, it emerges that Daam regulates Wnt signaling at the receptor level through RNF43, rather than at any event downstream in the Wnt pathway. To test this, we performed luciferase assays using the Wnt/β-catenin TOP-Flash reporter. In WT HEK293T cells, overexpression of N-Daam1, which aided RNF43-dependent degradation of Lrp6 (Fig. 3A), strongly inhibited the induction of luciferase activity by Wnt3a-conditioned medium (CM), while C-Daam1 had no effect (fig. S3D). However, N-Daam1 was unable to inhibit Wnt reporter activity in RZ DKO cells (*17*), indicating that Daam proteins mediate Wnt/β-catenin down-regulation through RNF43 (fig. S3D).

Daam1/2 knockout confers Rspo independence but fails to phenocopy RNF43/ZNRF3 knockout

To assess the consequences of Daam1/2 deletion in vivo in the mouse intestine, we generated a Daam1/2 double conditional KO mouse model (D1/2 cDKO), specifically for the small intestine by using the Villin-CreERT2 (Vil-CreER) transgenic system (fig. S4,

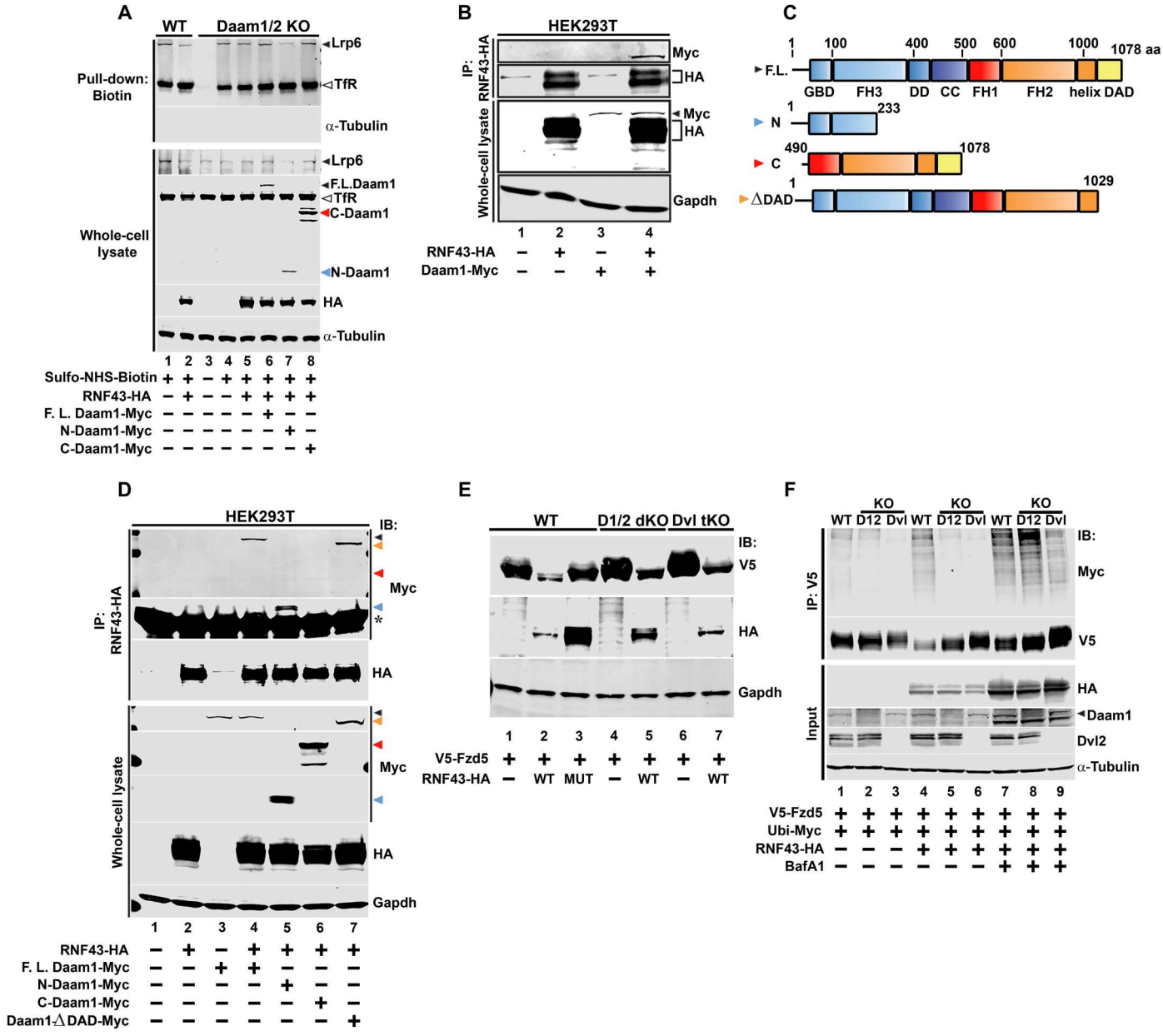

Fig. 3. Daam interacts with RNF43 through its N-terminal domain. (**A**) Western blot of representative cell surface protein biotinylation and pull-down assay on HEK293T cells transfected with indicated constructs, showing that Daam1/2 KO also prevents RNF43-dependent internalization of the Wnt co-receptor Lrp6. Note that N-Daam1 cooperates with RNF43 in reducing Lrp6 surface levels. Transferrin receptor (TfR) was used as a negative control. Colored arrowheads correspond to the different Daam1 constructs, as shown in (C). (**B**) Immunoprecipitation (IP) assay used to show the interaction between hemagglutinin (HA)-tagged RNF43 and Myc-tagged Daam1. (**C**) Schematic of the Daam1 full-length and deletion constructs used in this study to map the RNF43-interacting domain of Daam1. Daam1 architecture domain and relative amino acid position are indicated. GBD, Rho GTPase binding domain; FH3, formin homology 3 domain; DD, dimerization domain; CC, coiled-coil domain; FH1, formin homology 1 domain; FH2, formin homology 2 domain; Helix, an amphipathic helix involved in interaction with FH3 domain; DAD, diaphanous autoregulatory domain. (**D**) IP experiment showing that the N-terminal domain of Daam1 is required for RNF43 interaction. Colored arrowheads correspond to the different Daam1 constructs, as shown in (C), and indicate their migration position on the blot. (**E**) Western blots showing Frizzled degradation by RNF43 in WT, D1/2 DKO, and Dvl TKO HEK293T cells. (**F**) Western blot showing ubiquitin levels of Fzd5 in WT, D1/2, and Dvl mutant cells. α-Tubulin was used as a loading control in (A) and (F). Gapdh was used as a loading control in (B), (D), and (E).

A to C). We injected tamoxifen in 6- to 8-week-old, age-matched WT, D1/2 cDKO, and RZ cDKO mice to ablate Daam1/2 and RZ in the small intestinal epithelium, respectively. Two weeks after tamoxifen injection, small intestine sections were examined by Ki67 and lysozyme (Lyz) immunostaining to detect proliferative progenitor cells and PCs, respectively. As previously reported (*4*), RZ cDKO small intestinal epithelium showed clear hyperplasia with increased numbers of $Ki67^+$ proliferative cells and Lyz + PCs (Fig. 4, A and B). However, D1/2 cDKO epithelium only showed a mild increase of both cell types (Fig. 4, A and B), and there was no clear sign of hyperplasia in any of the examined sections.

We next tested whether cells from the newly generated D1/2 cDKO mouse showed Rspo independence, as we observed in Daam1/2 CRISPR mutants. To this end, we generated organoids from the small intestine of WT, D1/2 cDKO, and RZ cDKO mice after tamoxifen-induced deletion of Daam1/2 and RZ, respectively. All isolated organoids with different genotypes grew well in the WENR medium. When grown in WEN, only D1/2 and RZ cDKO organoids survived (Fig. 4C), confirming that D1/2 cDKO organoids acquired Rspo independence, as observed in the original D1/2 DKO CRISPR mutant organoids (Fig. 1H). Our organoid data also rule out any other defect in ISC maintenance, as D1/2 cDKO organoids could be maintained in vitro for multiple passages, as with the other lines. This was also supported by in situ hybridization analysis of intestinal tissue. *Olfm4* and *Axin2* expression patterns clearly confirmed the presence of ISCs and canonical Wnt signaling activity, respectively, in all three genotypes (Fig. 4D). Both D1/2 cDKO and RZ cDKO showed elevated *Axin2* signals, again confirming higher canonical Wnt activity (Fig. 4, D and E). However, we noted that $Wnt3^+$ PCs in D1/2 cDKO were not increased as much as in RZ cDKO, where PC hyperplasia was evident (Fig. 4, D and E), similar to Lyz immunostaining (Fig. 4A). We conclude that D1/2 cDKO renders ISCs more sensitive to Wnt ligand stimulation by compromising RZ-mediated negative feedback regulation. However, unlike RZ cDKO, D1/2 cDKO did not show a concomitant strong increase in the number of PCs.

Asymmetric role of Daam1/2 in noncanonical Wnt pathway for differentiation of Paneth cells

Daam1/2 is a well-characterized effector of the noncanonical Wnt/PCP signaling pathway, working downstream of another Wnt signaling regulator, Dvl (*18*, *19*). In particular, Daam proteins were shown to mediate Wnt/PCP-dependent reorganization of the actin cytoskeleton by activating Rho GTPases, a process required for gastrulation movements during vertebrate development (*18*, *19*). Recently, it has also been reported that PC differentiation involves activation of the Wnt/PCP pathway (*25*). This prompted us to test whether the difference in PC number between D1/2 and RZ cDKO small intestines was caused by the lack of Wnt/PCP signaling.

Hence, we monitored the activation of the Wnt/PCP signaling pathway upon stimulation with Wnt5a, a well-known noncanonical Wnt ligand, in WT and D1/2 DKO HEK293T cells. Dvl phosphorylation was intact in both WT and D1/2 DKO HEK293T cell lines, indicating proper Wnt/PCP activation upstream of Daam1/2 upon Wnt5a treatment (Fig. 5A and fig. S5A). However, downstream signaling events were compromised as we could not observe any Wnt5a-dependent elevation of active Rho protein level in D1/2 DKO HEK293T cells (Fig. 5A), in agreement with previous reports (*18*). Curiously, active Rho levels in D1/2 DKO cells remained steadily higher than in WT cells, for unknown reasons. It has been demonstrated that Daam recruits the GTPase activating protein (GAP) SRGAP2 (*26*). It is possible that Daam1/2, in complex with SRGAP2 or other GAPs, promotes the GTPase activity of Rho, thus actively controlling active (GTP-bound) Rho levels, which would increase in the absence of Daam1/2.

In addition, molecular imaging of F-actin dynamics using LifeAct-GFP or phalloidin also showed that D1/2 DKO HEK293T cells lack Wnt5a stimulation-dependent cytoskeleton rearrangement and filopodia formation (Fig. 5B and fig. S5, B to D), a hallmark of Wnt/PCP defect (*27*–*29*). Together, these data indicate that D1/2 KO cells show defects in the Wnt/PCP pathway, in agreement with published work. In contrast, as shown above with the lack of negative feedback regulation by RNF43, canonical Wnt signaling activity was enhanced in the D1/2 DKO HEK293T cells as they showed a higher level of unphosphorylated active β-catenin level both at a steady state and upon Wnt3a stimulation (Fig. 5C). We also confirmed elevated expression of canonical Wnt target genes, both in HEK293T cells and mouse small intestinal organoids, by reverse transcription quantitative polymerase chain reaction (RT-qPCR) (Figs. 5D and 6A). To test whether our findings on Wnt/β-catenin modulation by Daam1/2 could be extended to other systems, we resorted to the frog model *Xenopus laevis*. During *Xenopus* development, a Wnt/β-catenin gradient is instrumental in determining the anteroposterior body axis, where Wnt activity is lower in the anterior and higher in the posterior (*30*). Because of this, overexpression of Wnt inhibitors in frog embryos causes enlargement of the head and anterior structures (anteriorization) (*31*, *32*), while Wnt activation induces head loss (posteriorization) (*33*). To test whether D1/2 knockdown could mimic a Wnt activation phenotype, we performed a D1/2 morpholino (MO)–mediated knockdown experiment (fig. S6, A to C). When injected into the dorsal blastomeres of four-cell stage *Xenopus* embryos (fig. S6D), Daam1/2-specific MOs synergistically reduced head development compared to WT controls (fig. S6, E to I), phenocopying canonical Wnt overactivation (fig. S6H).

Since Daam1/2 KO impairs Wnt/PCP signaling (Fig. 5, A and B), we checked the consequence of the Wnt/PCP defect on PC differentiation using mouse small intestinal organoids. Lyz immunostaining (Fig. 6B and fig. S7A) and UEA1 flow cytometry analysis (Fig. 6C) showed that the number of PCs was decreased in D1/2 cDKO organoids, as compared to WT and RZ cDKO organoids. Consistent with in vivo data (Fig. 4A) (*4*), RZ cDKO organoids showed typical PC hyperplasia (Fig. 6, B to E, and fig. S7A). Furthermore, WT intestinal organoids expressing a fluorescent reporter under the regulation of the lysozyme promoter (*Lyz1::mRuby*) showed a higher number of PCs when treated with Wnt5a, suggesting that activation of noncanonical Wnt signaling is sufficient to stimulate PC differentiation (Fig. 6D and fig. S7B). Fluorescence-activated cell sorting (FACS) analysis on Lyz1::mRuby organoids also confirmed that treatment with Wnt5a induced an increase in PC number (fig. S7, C to E). Noncanonical Wnt signaling is involved in a variety of cancers, including chronic lymphocytic leukemia (*34*), and inhibitors of key components of the pathway, such as casein kinase 1ε (CK1ε), show potential for treating hematological cancers (*35*). Treatment with compound PF-4800567 (hereafter, PF48), a potent and selective inhibitor of CK1ε, led to a decrease

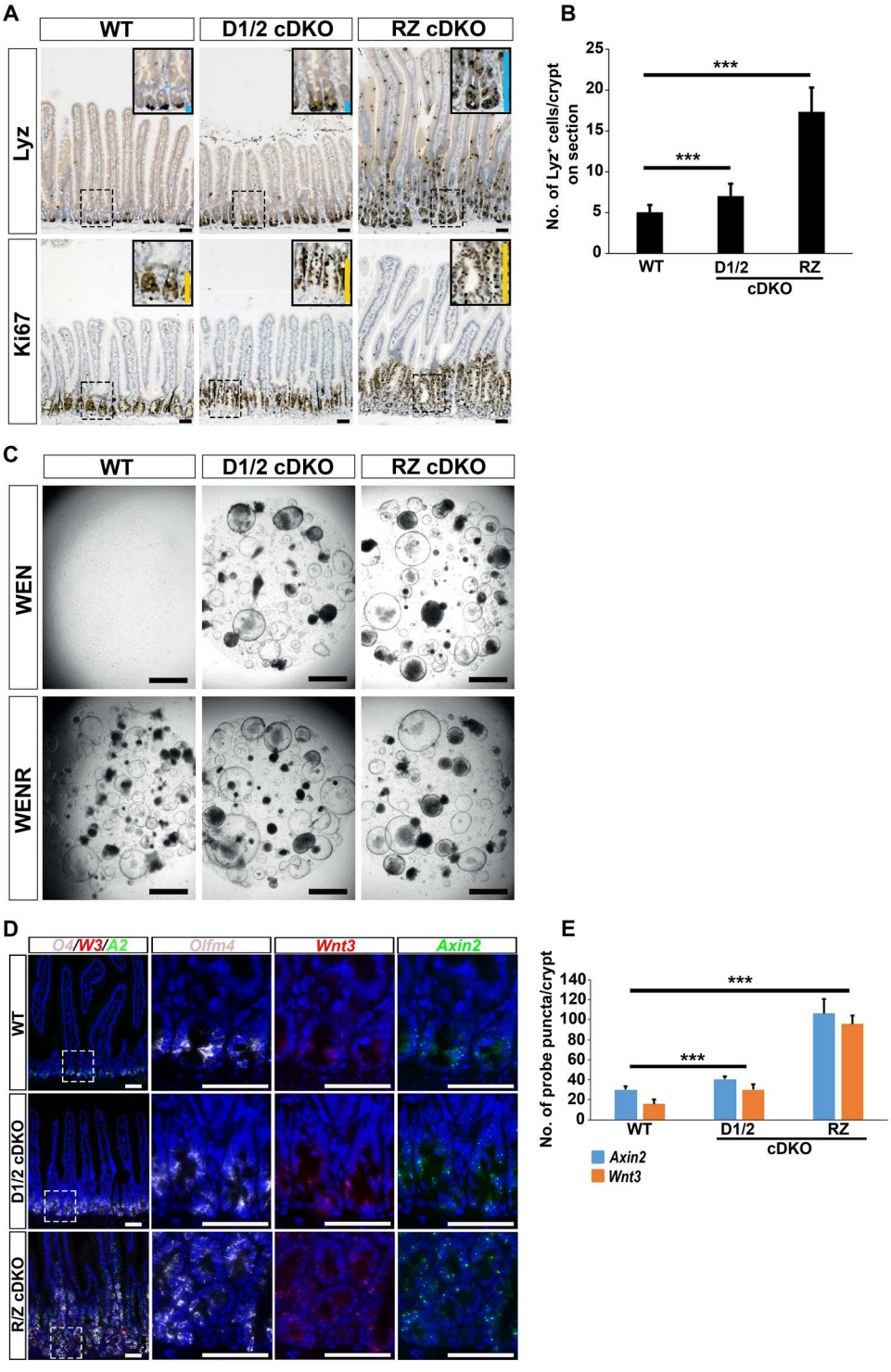

Fig. 4. Daam1/2 cDKO mice show a milder phenotype than RZ cDKO, despite maintaining Rspo1 independence. (**A**) Small intestine histological sections from WT, D1/2, and RZ conditional double KO mice stained for lysozyme (Lyz), a PC marker, and Ki67, used as a proliferation marker. Insets show magnification of dash-boxed areas. The extent of Lyz-positive Paneth zones and Ki67-positive proliferative zones are indicated by blue and yellow sidebars, respectively. (**B**) Bar plot representing experiment quantification, showing mean values and SD. *P* values (D1/2: 0.0009; RZ: 5.42×10^{-10}) were calculated using an unpaired two-tailed *t* test. (**C**) Organoids derived from WT, D1/2, and RZ cDKO mice, showing that D1/2 and RZ mutant organoids can survive in the absence of R-spondin, unlike WT organoids. (**D**) RNAscope in situ hybridization analysis with probes targeting *Olfm4* (*O4*, stem cell marker), *Wnt3* (*W3*, PC marker), and *Axin2* (*A2*, canonical Wnt target gene). White dashed boxed areas shown in the left "merge" panels are enlarged and shown on the right as single probe staining. Scale bars, 50 μm [(A) and (D)] and 1000 μm (C). (**E**) Bar plot representing experiment quantification, showing mean values and SD. *P* values were calculated using an unpaired two-tailed *t* test. *P* values: (D1/2 Axin2: 2.03×10^{-10}; Wnt3: 1.93×10^{-08}); (RZ Axin2: 2.97×10^{-18}; Wnt3: 6.25×10^{-24}).

in PCs while the Rho kinase (Rock) inhibitor Y-27632 did not (fig. S7, C to E).

To further confirm the role of Wnt/PCP signaling in PC differentiation, we performed single-cell RNA sequencing (scRNA-seq) analysis of WT, RZ cDKO, and D1/2 cDKO organoids that were cultured in WENR conditions. In total, we analyzed 8000 (WT), 13,000 (RZ cDKO), and 9000 (D1/2 cDKO) cells, and identified five main clusters in Uniform Manifold Approximation and Projection (UMAP) (Fig. 7A and fig. S8, A to C). These clusters consisted of revival stem cells, *Lgr5*$^{+}$ stem cells, proliferating cells, enterocytes, and mature secretory lineage cells. Because of the use of high canonical Wnt stimulation in organoid culture medium, progenitor cell populations were highly represented; this is a favorable condition that allowed us to gain insights into the initial commitment to

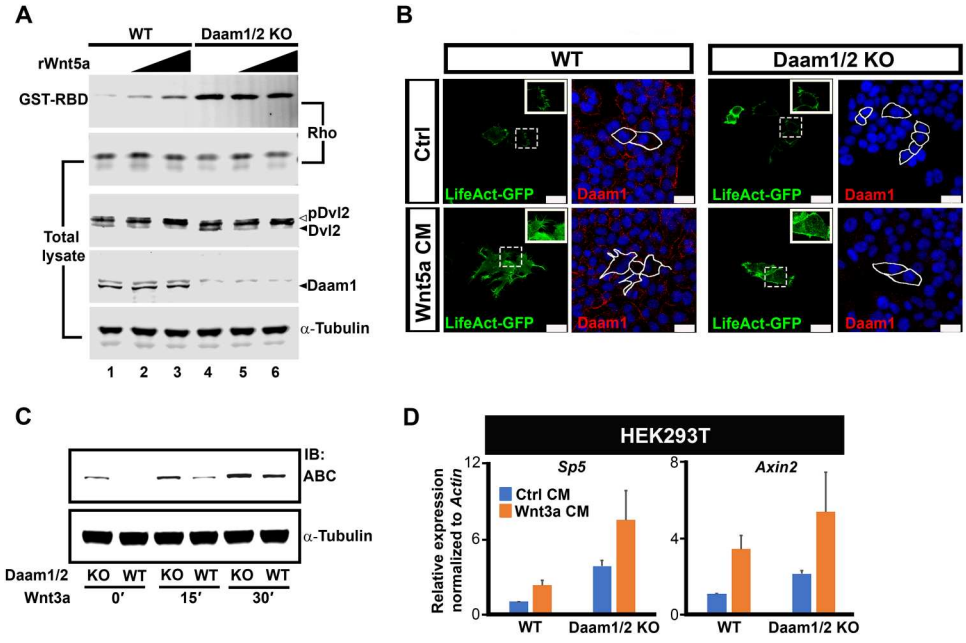

Fig. 5. Daam knockout impairs noncanonical Wnt while enhancing canonical Wnt signaling. (**A**) Active Rho pull-down assay. WT and D1/2 KO cells were treated with recombinant Wnt5a (0, 200, or 400 ng/ml) for 30 min at 37°C before Western blot analysis. White and black arrowheads point to phosphorylated and unphosphorylated Dvl2, respectively, which served to monitor for Wnt5a activity. Daam1 immunoblot was used to confirm its absence in D1/2 KO cells. (**B**) WT and D1/2 KO HEK293T cells transfected with LifeAct-GFP were treated with Wnt5a CM for 2 hours at 37°C, before immunofluorescence analysis. Insets show magnification of the dash-boxed area. White lines indicate transfected cell location among nontransfected cells. Scale bars, 20 μm. (**C**) Western blot comparing levels of active β-catenin in WT and D1/2 KO HEK293T cells. Cells were treated with Wnt3a CM for the indicated time, before analysis. α-Tubulin was used as a loading control in (A) and (C). (**D**) Reverse transcription quantitative polymerase chain reaction (RT-qPCR) analysis of canonical Wnt target genes *Sp5* and *Axin2* on WT and D1/2 KO cells treated overnight with Wnt3a CM. Expression levels are normalized to *Actin* mRNA. Error bars represent SD across three biological replicates.

different cell lineages of the progenitor cell populations. The number of $Lgr5^+$ cells was comparable among all three genotypes with a small decrease observed in D1/2 cDKO organoids, which was compensated by a concomitant increase in the fraction of revival stem cells (Fig. 7B). In D1/2 cDKO organoids, the most significantly affected populations were the mature secretory cell types (Fig. 7B). Likewise, $Neurog3^+$ and $Tff3^+$ secretory lineage progenitor cells (Fig. 7C) were missing in D1/2 cDKO organoids. $Dll1^+$ early secretory progenitors were still present in D1/2 cDKO organoids (Fig. 7C), suggesting that the first binary commitment to the secretory lineage by Notch signaling is not affected by Daam1/2 KO (Fig. 7D). We also observed decreased levels of *Clca3b* and *Cfap126/Flattop* [*Fltp*, a known Wnt/PCP target gene (*25*, *36*)] (Fig. 7, C, E, and F), as well as of the PC markers *Defa24* and *Defa17* (Fig. 7C). The number of $Dclk1^+$ tuft cells was significantly increased in the D1/2 cDKO organoids (Fig. 7C), probably as a result of the block toward other secretory lineages among committed $Dll1^+$ cells. These results were also confirmed through pseudo-bulk RNA-seq analysis, as shown in fig. S9 (A to G). These data provide the first genetic evidence that Wnt/PCP is involved in secretory lineage specification, particularly PC differentiation, as predicted by previous work (*25*). In agreement with the data presented here and from others (*25*), we propose the following stepwise binary fate decision model for intestinal cell specification: First, Notch signaling directs the choice between absorptive and secretory (*Dll1*+) lineages; then, Wnt/PCP signaling regulates differentiation between tuft and other secretory lineages (Fig. 7D).

Last, our analysis of the differentiation pattern of D1/2 cDKO intestinal epithelial cells provides a clear explanation for why we did not observe a similar PC hyperplasia as observed in the RZ cDKO intestine (Fig. 4A). We previously showed that introducing Math1 or Wnt3 cKO into a RZ cDKO genetic background prevented PC formation and produced a strongly alleviated phenotype, despite maintaining Rspo independence and Wnt hypersensitivity (*37*). D1/2 cDKO leads to the same alleviated phenotype by the unexpected combination of Rspo independence and PC defects, caused by the asymmetric regulation of canonical (up) and noncanonical (down) Wnt signaling by Daam1/2 KO.

DISCUSSION

Using cell cultures, organoids, and mouse models, we have demonstrated that Daam1 and Daam2 are novel downstream regulators of RZ in the small intestine, which mediate endocytosis of ubiquitinated Fzd. A similar endocytic function for Daam1 has been previously reported and shown to be important for ephrinB signaling in the zebrafish notochord (*38*). Of note, interaction with ephrinB occurred via the N-terminal domain of Daam1 (*38*), analogous to the RNF43-Daam1 interaction uncovered here. Similarly, Daam1 was shown to interact through its N-terminal domain with β-arrestin2, a protein regulating endocytosis and Wnt/PCP signaling during *Xenopus* convergent extension (*39*). We thus speculate that our work uncovers a more general role for Daam proteins in cell signaling regulation via endocytosis, a fundamental process in Wnt

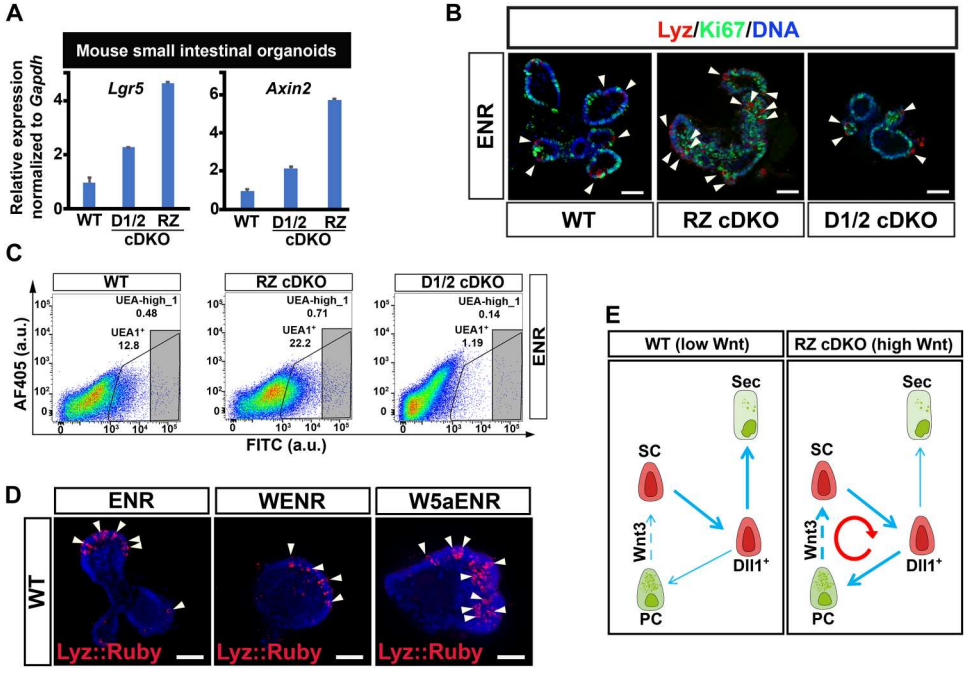

Fig. 6. Daam knockout in small intestinal organoids prevents the efficient generation of Paneth cells. (**A**) RT-qPCR analysis of canonical Wnt target genes *Lgr5* and *Axin2* on WT, D1/2, and RZ cDKO mouse small intestinal organoids. Expression levels are normalized to *Gapdh* mRNA. Error bars represent SD across three biological replicates. (**B**) Organoids derived from WT, RZ, and D1/2 cDKO mice cultured in ENR medium and stained for lysozyme and Ki67. Arrowheads point at PCs (Lyz$^+$, in red). (**C**) FACS analysis of organoids from indicated mouse genotypes, stained with fluorescein isothiocyanate (FITC)–labeled *Ulex europaeus* agglutinin 1 (UEA1). (**D**) Confocal imaging of *lysozyme::mRuby* WT SI organoid reporter line, expressing mRuby red fluorescent protein in PCs. Organoids were cultured in ENR, and WENR on Wnt5a-containing ENR. Scale bars, 50 μm [(B) and (D)]. (**E**) Schematic showing PC ISC double-positive feedback in normal homeostatic and Wnt high conditions (such as in RZ cDKO intestine). a.u., arbitrary units.

signaling (*40*, *41*), perhaps shared by other members of the formin superfamily (*42*).

We have also confirmed that Daam1/2 plays an important role in the noncanonical Wnt pathway as a downstream effector of Dvl. Hence, loss of Daam1/2 enhances canonical Wnt signaling while reducing Wnt/PCP signaling (see model in Fig. 8, A and B). In contrast, RZ negatively regulates both canonical and noncanonical Wnt, by targeting canonical Wnt receptors Fzd and Lrp6 (*4*, *5*), as well as noncanonical Wnt components Ror1/2 and Vangl1/2 (*17*) for degradation, such that its loss causes enhanced signaling in both pathways (Fig. 8A) (*43*–*45*). Because of this difference, RZ cDKO intestine showed hyperplasia with overproduction of PCs, whereas D1/2 cDKO intestine displayed an alleviated phenotype, characterized by a lack of efficient PC specification when compared to RZ cDKO (Fig. 8C). A similar phenotype has been observed in *RZ;Math1* and *RZ;Wnt3* TKO intestine (*37*). Math1 is an important transcription factor for PC specification and Wnt3 is the canonical Wnt ligand expressed by PCs. Knocking out Math1 and Wnt3 in the RZ background compromises PC formation and function, respectively. As a result, *RZ;Math1* and *RZ;Wnt3* show much less Lyz$^+$ PCs or Ki67$^+$ proliferative progenitors as compared to RZ DKO (*37*), but still slightly higher than WT mouse intestines, in close analogy to what we have shown here for D1/2 DKO. Our data unveil an unexpected additional binary fate decision step regulated by Wnt/PCP signaling, after the well-known primary fate decision between absorptive and secretory lineages regulated by Notch signaling (*1*). This Wnt/PCP-regulated fate determination step seems to govern secretory cell differentiation between tuft cells and other secretory cell types, including PCs (Fig. 7D). In D1/2 cDKO intestine and organoids, secretory lineage differentiation is heavily compromised, particularly at the expense of PCs, while increasing the production of tuft cells, which are usually the rarest population in the gut epithelium.

PCs represent a key epithelial cell population that provides neighboring stem cells with essential niche factors, especially Wnt3. Such epithelial Wnt-producing cells can be an important protumorigenic niche for tumorigenic stem cells that are still dependent on Wnt ligands for their maintenance and growth (e.g., RZ mutants or Rspo fusion–bearing mutants). PC hyperplasia in RZ tumors is known to create a positive feedback loop that sustains Wnt-addicted tumor cells via the massive production of Wnt-secreting cells (*37*) (Fig. 8C). For this reason, porcupine inhibitors have received particular attention as they can be used to inhibit Wnt secretion from the tumorigenic niche (*37*). Our data suggest another vulnerable point since inhibiting noncanonical Wnt signaling can have a similar effect by altering the secretory lineage specification. In conclusion, our study not only provides genetic evidence for the role of Wnt/PCP signaling in intestinal secretory lineage specification but also opens up new therapeutic avenues to treat Wnt-addicted cancers.

Although we show a clear impact for noncanonical Wnt signaling in PC generation, we should also highlight some limits in our study. One of these is that our analysis on noncanonical Wnt signaling in vivo and on organoids is limited to a few readouts. Note

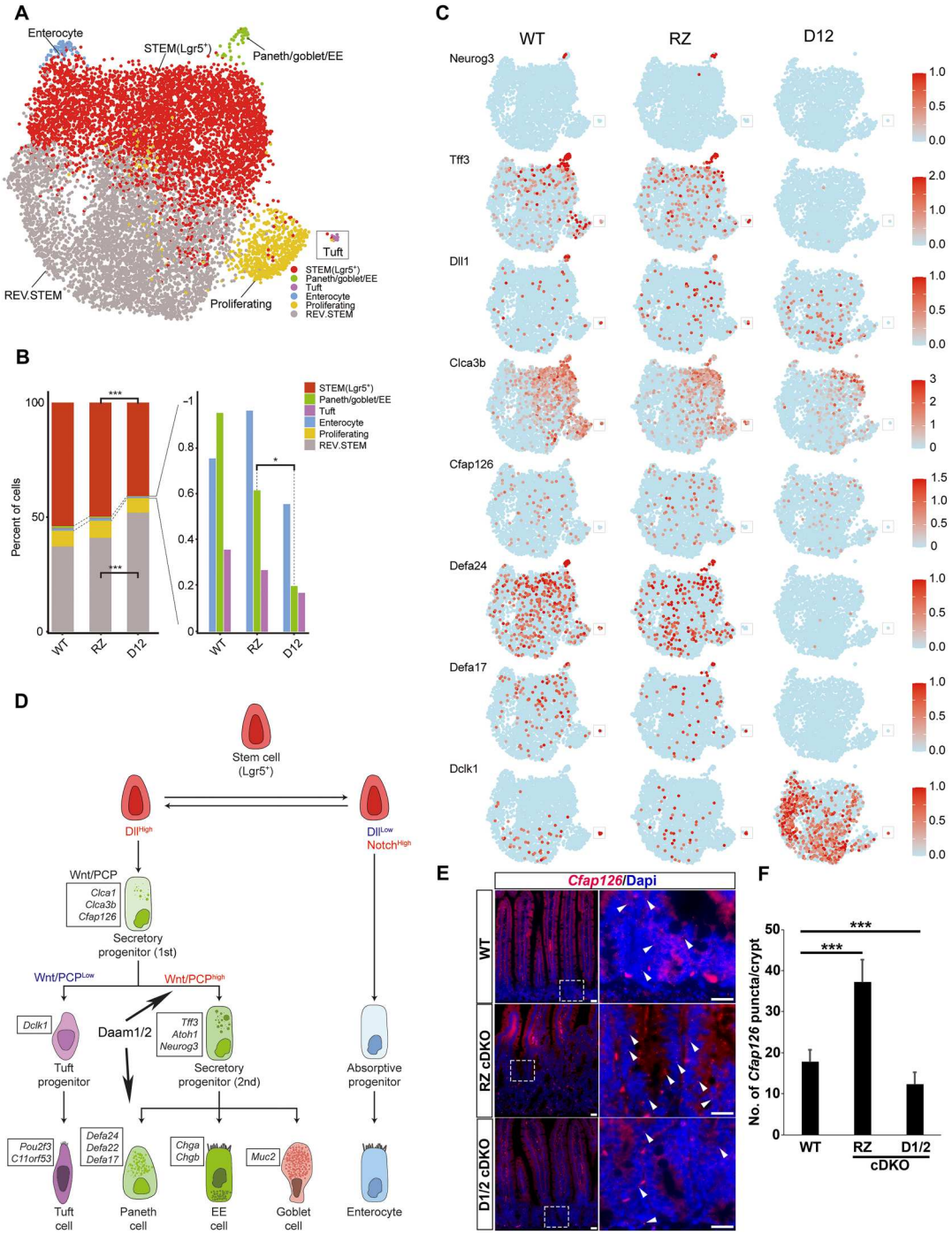

Fig. 7. scRNA-seq analysis on WT, RZ, and D1/2 cDKO organoids shows that Daam1/2 is required for Paneth cell differentiation. (**A**) Integrated Uniform Manifold Approximation and Projection (UMAP) cluster map including WT, RZ, and D1/2 samples. (**B**) Cell-type composition of WT, RZ, and D1/2 organoids. *P* values were calculated by Fisher's exact tests. Corrected *P* values were described as $*P < 0.01$ and $***P < 0.001$. (**C**) Expression pattern of selected cell type markers on UMAP clusters from individual samples. The red color indicates the maximum expression level, while the blue color indicates the minimum expression level for each gene. (**D**) Cellular flow chart showing the stepwise commitment from Lgr5^{+} stem cells. Dll^{high} progenitors can generate secretory cells including tuft, Paneth, enteroendocrine (EE), and goblet cells, while Dll^{low} will only generate enterocytes. Among Dll^{high} progenitors, only cells with active Wnt/PCP signaling can mature into Paneth, EE, and goblet cells. Note that Daam1/2 activity is positioned after the first secretory progenitor specification, where it regulates Wnt/PCP and consequently PC differentiation (arrows). (**E**) In situ hybridization using an RNAscope probe specific for *Cfap126* (*Fltp*) in the small intestinal crypts of WT, RZ, and D1/2 cDKO mice. The right panels are the enlargement of areas included in the dash boxes on the left. White arrowheads indicate the fluorescent signal from single mRNA transcripts (red puncta). Note the decrease in *Cfap126/Fltp* expression in D1/2 KO mice. Scale bars, 20 μm. (**F**) Bar plot showing quantification of *Cfap126/Fltp* probe puncta shown in (E). Mean values and SD are shown, and *P* values were calculated with unpaired two-tailed *t* test. *P* values: (RZ: 1.57 × 10−08); (D1/2: 0.00046).

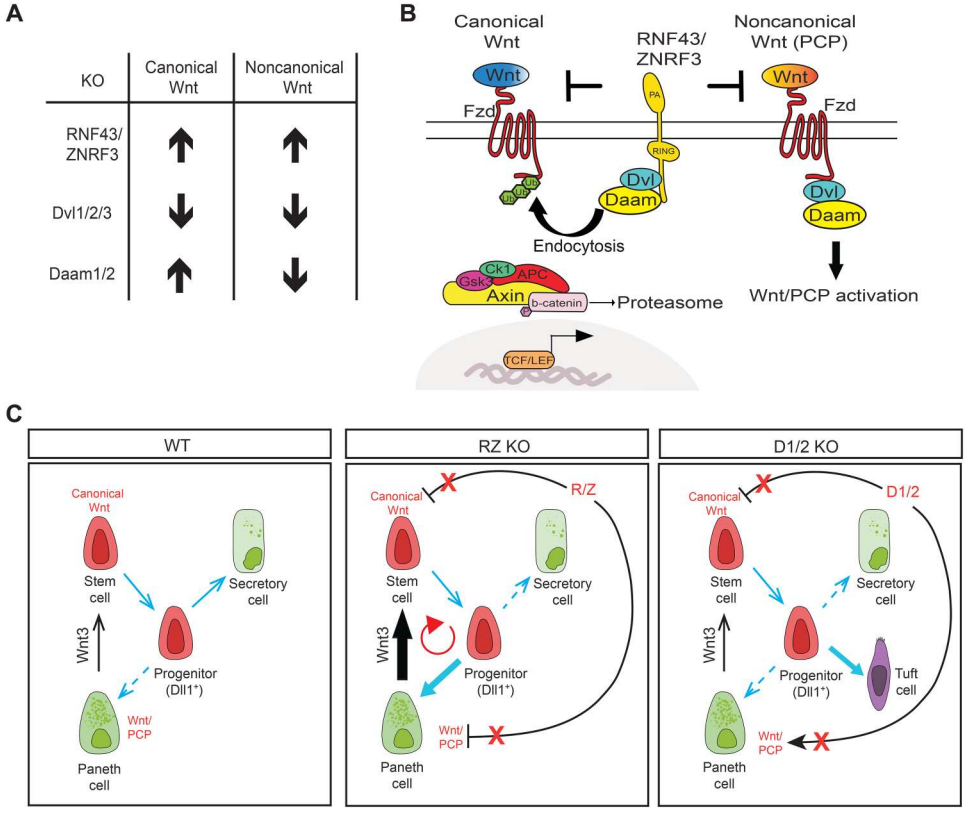

Fig. 8. Model summarizing the role of Daam1/2 in the context of Wnt signaling and Paneth cell differentiation. (**A**) Diagram showing the effects of RNF43, Dvl1/2/3, and Daam1/2 KOs on canonical and noncanonical Wnt signaling. RNF43 KO increases both pathways, due to the increase of Frizzled receptors. Conversely, triple KO of Dvl1/2/3, a common effector of canonical and noncanonical Wnt, leads to a decrease in both. Unlike RZ and Dvl1/2/3, Daam1/2 shows an asymmetric regulation of the two Wnt pathways as the KO of Daam1/2 triggers canonical Wnt activation while inactivating noncanonical Wnt signaling. (**B**) Diagram showing Daam1/2 within the different Wnt pathways. Left: Daam1/2 interacts with RNF43, allowing endocytosis of Fzd receptors ubiquitinated by RNF43. This terminates the Wnt/β-catenin signal. Right: Daam1/2 interacts with Dvl, regulating positively downstream events of the Wnt/PCP pathway. (**C**) Comparison between the effects of RZ and D1/2 KO in PC differentiation. RZ mutant mice undergo rapid intestinal adenoma formation caused by ISCs and Wnt-secreting PC co-hyperplasia. The absence of RZ boosts both canonical and noncanonical Wnt, increasing the number of PCs. In turn, this leads to more Wnt3 production, sustaining high stem cell proliferation, which is stimulated to differentiate into more PCs (rather than other secretory cells) because of the high levels of Wnt/PCP. On the other hand, Daam1/2 mutants show a completely alleviated phenotype, thanks to the noncanonical Wnt defect that prevents efficient PC differentiation, thereby reducing Wnt3 ligands in the microenvironment.

however that very little is known about target genes directly activated by Wnt/PCP, and among these, *fltp* was established only recently as a bona fide noncanonical Wnt target in the mammalian intestine (*25*). Furthermore, because we analyzed our Daam1/2 cDKO mice shortly after tamoxifen induction, we do not know the long-term consequences of noncanonical Wnt impairment in the physiology of the adult intestine. At least, we noted that Daam1/2 cDKO small intestinal organoids could be passaged many times, similarly to WT organoids when supplemented with exogenous Wnt3a. Future work will help clarify the role of Daam1/2 genes in the long-term maintenance of intestinal epithelium in vivo.

MATERIALS AND METHODS

Experimental design

The prespecified objectives of this study were to determine the role of Daam proteins in the regulation of Wnt/β-catenin signaling by RNF43, as well as their role in ISC homeostasis. To address these key questions, a combination of biochemical, immunostaining, FACS, RT-qPCR, and various conditional genetic KO or CRISPR-Cas9 KO models was used to determine the function of Daam1/2 in different systems: cell culture, small intestinal organoids, and in vivo models (*Xenopus* embryos and mice).

Mouse husbandry and generation of conditional knockouts

Daam1tm1a(EUCOMM)Hmgu and Daam2tm1a(KOMP)Wtsi chimeras were generated by blastocyst microinjection. Chimeras were crossed with the Villin-CreERT2 (Vil-CreERT2) mouse line to generate the conditional *Vil-CreERT2;Daam1*$^{fl/fl}$, *Vil-CreERT2;Daam2*$^{fl/fl}$, and *Vil-CreERT2;Daam1*$^{fl/fl}$*;Daam2*$^{fl/fl}$ lines. The *Vil-CreERT2;RNF43*$^{fl/fl}$*;ZNRF3*$^{fl/fl}$ mouse line was included as a positive control. To induce Cre recombinase, 2 mg of tamoxifen in corn oil per 20 g of body weight or corn oil alone for negative control animals were injected at age 8 to 12 weeks. Both male and female mice were included in the experiments. Small intestine crypts were isolated, and organoids were established for further in vitro experiments, as described below. All mice were euthanized 2 weeks after Cre induction. Standard light/dark cycle, temperature, and humidity parameters were used by the mouse facility to maintain all mouse

lines. All animal experiments adhered to the guidelines of the Austrian Animal Care and Use Committee.

Small intestinal organoid establishment and maintenance

Small intestinal crypt isolation and organoid establishment were reported previously (*4*, *37*). Briefly, mouse small intestinal crypts were isolated by applying Gentle Cell Dissociation Reagent from STEMCELL technologies at room temperature (RT) for 20 min. About 100 to 150 isolated crypts per well were seeded in Matrigel with ENR (Egf, Noggin, and R-spondin1) or WENR (Wnt3a-containing ENR) + nicotinamide (WENR+Nic) culture medium composed of advanced Dulbecco's modified Eagle's medium (DMEM)/F12 supplemented with penicillin-streptomycin, 10 mM Hepes (Gibco), GlutaMAX (Gibco), 1× B27 (Life Technologies), 10 mM nicotinamide (MilliporeSigma; used only in WENR), 1.25 mM *N*-acetylcysteine (Sigma-Aldrich), mouse Epidermal Growth Factor (mEGF; 50 ng/ml; PeproTech), mNoggin (100 ng/ml; PeproTech), 10% R-spondin1 CM, 50% Wnt3A CM (only in WENR), and 10 mM ROCK inhibitor (Tocris). Established organoids were routinely passaged at 1:3 to 1:5 ratios every week and maintained in a culture medium without ROCK inhibitor.

Organoid single-cell analysis

To induce gene recombination in *Vil-CreERT2;Daam1/2* double conditional KO (D1/2 cDKO) and *Vil-CreERT2;RNF43-ZNRF3* double conditional KO (RZ cDKO) small intestinal organoid lines, 4-hydroxytamoxifen (1 μg/ml) was added in WENR+Nic (Wnt, Egf, Noggin, R-spondin1 + nicotinamide) organoid culture medium. After recombination, D1/2 and RZ mutant organoids were cultured in the WEN+Nic medium for selection purposes, as only successfully recombined mutant cells survive in the absence of Rspo1. WT, D1/2 cDKO, and RZ cDKO organoids were maintained in regular WENR+Nic (WT) or WEN+Nic (D1/2 and RZ cDKO) culture medium for 10 days before single-cell analysis. Three days before single-cell analysis, organoids were passaged at a 1:3 ratio. For analysis, organoids were mechanically and chemically dissociated and prepared for library generation and sequencing by Vienna BioCenter Next Generation Sequencing Facility. WT (8,000), RZ cDKO (13,000), and D1/2 cDKO (9,000) cells were analyzed and obtained sequencing data were processed as described below.

scRNA-seq data preprocessing

To generate count matrices for each organoid sample such as WT ("WT_WENR"), RNF43/ZNRF3 double KO (RZ_WEN), and Daam1/Daam2 double KO (Daam:WEN), Cell Ranger (v6.1.1) (*46*) was used with default option and mouse reference ("refdata-gex-mm10-2020-A") provided in 10x Genomics. On the basis of the Seurat pipeline (v4.1.0) (*47*), we generated analytic objects from each gene-by-cell matrix from "filtered_feature_bc_matrix" of Cell Ranger, we first filtered out poor-quality cells with less than 4,000 and more than 40,000 unique molecular identifiers (UMIs), more than 13% mitochondrial genes, and more than 4,000 detected genes for WT_WENR and RZ_WEN samples. In particular, for the Daam:WEN sample, we applied partially different criteria to discard poor-quality cells with more than 50,000 UMIs and more than 5,000 detected genes. After the quality control (QC) step, we had 3828 cells (WT_WENR), 4342 cells (RZ_WEN), and 3257 cells (Daam:WEN). Then, we sequentially conducted NormalizeData (log-normalization) and FindVariableFeatures ("vst" method, 2000 features) functions of the Seurat pipeline for each sample. To select a singlet, DoubletFinder_v3, which is a recent version of DoubletFinder (*48*), was conducted with default parameters. Using cell cycle markers derived from the AnnotationHub R package (v3.4.0) with "*Mus musculus*," "EnsDb" for S and G2/M phases, we calculated cell cycle scores via CellCycleScoring function and regressed out based on the scores such as "S.Score" and "G2M.Score" on Seurat pipeline. After merging three count objects and storing each object in a sample category, we performed principal components analysis (PCA) with the RunPCA function to prepare harmonization which is one of the batch reduction methods. The merged object was harmonized through the RunHarmony function with "Sample" as a biological factor and 30 PCs (*49*). On the basis of the dimensionally reduced object, we identified clusters through sequential procedures such as RunUMAP, FindNeighbors ("k.param" is 25), and FindClusters ("resolution" is 0.75, Louvain algorithm) with 30 harmony PCs.

scRNA-seq data analysis

To annotate cell types in the dataset, we used cell type markers described in fig. S8. Using the expression profile of clusters, the clusters have been combined to reflect that intestinal organoids cultured in conventional media consist of a large proportion of stem cells and a small proportion of fully differentiated cells (*50*). Because genetic changes may affect cell homeostasis and transcriptomic changes of cell type markers, we annotated cell types based on gene expression in WT_WENR. To generate dot plots for each sample origin, expression patterns of each gene within cells corresponding to sample and cluster instances were used. Using the dittoBarPlot function in the dittoSeq R package (v1.6.0) (*51*), we generated cell type proportion in each sample. The statistical significances for the difference of a cell type between samples were estimated through Fisher's exact test. We showed the expression pattern of each gene on UMAP clusters for combined samples and individual samples based on UMAP coordinates and expression levels.

Pseudo-bulk RNA-seq analysis

From scRNA-seq data, aggregation of UMI counts from a group of cells has been used to observe differential gene expressions across clusters or sample-wise. To capture the global effect of genetic differences in the transcriptome, we adopted a pseudo-bulk approach with 10 pseudo-samples from each of the scRNA-seq count matrices with QC-passed cells according to WT_WENR, RZ_WEN, and Daam:WEN samples. Each sample has a gene-by-pseudo-sample count matrix and each column (i.e., a pseudo-sample) contains the aggregated UMI counts for the corresponding genes from the same number of randomly selected cells. We used the DESeq2 (*52*) R package to normalize UMI counts. For each gene, we compared log-scaled normalized expression levels from samples and estimated statistical significance with the Mann-Whitney *U* test and Kruskal-Wallis test by using the "stat_compar_means" function on "ggpubr" R package (v0.4.0).

Organoid electroporation

Small intestinal organoids were electroporated following a previously established protocol (*16*). Two days before electroporation, the culture medium was replaced from WENR+Nic to EN+Nic in the presence of ROCK inhibitor and the Gsk3 inhibitor CHIRON

99021. One day before electroporation, 1.25% v/v dimethyl sulfoxide was added to the culture medium. On the day of electroporation, organoids were dissociated into small clusters by TrypLE treatment, and electroporation was performed in 400 μl of BTXpress buffer (Havard Apparatus) with 12.5 μg of DNA using a NEPA21 Electroporator (NEPA Gene). For CRISPR-Cas9–mediated KO, organoids were electroporated with CRISPR concatamer vectors containing gene-specific gRNAs in combination with a Cas9 expression plasmid (Addgene, #41815) at a 1:1 ratio. The electroporated organoids were seeded in Matrigel and cultured with EN medium in the presence of Nic and ROCK inhibitor. Two days later, the post-electroporation culture medium was replaced by a regular culture medium (ENR or WENR). DNA oligos and primers used to generate and analyze CRISPR KO organoids are listed in table S2.

Generation of a Paneth cell reporter SI organoid line

SI organoids expressing tamoxifen-inducible Cas9 were established from *Vil-CreERT2;Rosa26*$^{LSL\text{-}Cas9}$ mice. These organoids were co-electroporated with a plasmid containing *Lysozyme1* (*Lyz1*) single guide RNA (sgRNA) for *Lyz1* and a Golden Gate–generated targeting vector containing the coding sequence of *2A peptide–mRuby* red fluorescent protein, followed by a phosphoglycerate kinase promoter (PGK)–driven blasticidin resistance gene and flanked by homology arms of 48 base pairs of length that are homologous to the region immediately up- and downstream of the Lyz1 stop codon. After electroporation, organoids were selected with blasticidin (100 μg/ml) for 6 to 7 days. Hence, single surviving organoids were manually isolated to generate monoclonal lines and genotyped to confirm the correct integration of *mRuby* in *Lyz1*. For Wnt5a treatment, Lyz1::mRuby organoids were seeded in ENR, WENR, or W5aENR, where recombinant Wnt5a protein (rWnt5a, R&D Systems) is added to ENR at a final concentration of 200 ng/ml. Organoids were cultured for 5 days before imaging analysis. Media were refreshed every 2 days.

Immunofluorescence of intestinal organoids for FACS analysis

Both WT and *Lyz1::mRuby* small intestinal organoids were collected from the Matrigel domes and gently dissociated mechanically with a P1000 or a P200 pipette and transferred to 1.5-ml tubes. The mixtures were spun down at 600*g* for 3 min and the supernatant was removed. The organoid/cell pellets were resuspended in 500 μl of TrypLE Express Enzyme (Gibco, 12604013) and incubated at 37°C for 5 min. After incubation, the mixtures were pipetted up and down a few times to aid the dissociation into single cells. The mixtures were then spun down at 600*g* for 3 min and the supernatant was removed. The cell pellets were resuspended in FACS buffer [2% fetal bovine serum (FBS) and 2 mM EDTA in phosphate-buffered saline (PBS)] for washing and spun down at 600*g* for 3 min. After removing the supernatant, the pellets were resuspended in an antibody mixture containing UEA1 (1:500) in 2% FBS in PBS and incubated on ice for 1 hour. The mixtures were then spun down at 600*g* for 3 min and washed three times with the FACS buffer before being passed through a 40-μm filter. Cells were analyzed using a BD-LSR Fortessa flow cytometer (BD Biosciences), and the flow cytometry data were analyzed using FlowJo software (BD Biosciences).

Immunohistochemistry and RNAscope in situ hybridization

All immunohistochemical (IHC) staining experiments on mouse intestinal sections were performed by the IMBA Histology Facility at Vienna BioCenter Core Facilities. All samples were incubated in 3% H_2O_2 in blocking solution {2% bovine serum albumin (BSA), 5% goat serum, 0.3% Triton X-100 in PBS [137 mM NaCl, 2.7 mM KCl, 10 mM Na_2HPO_4, and 1.8 mM KH_2PO_4 (pH 7.4)]} at RT for 10 min and further incubated in blocking solution at RT for 1 hour. Sections were incubated overnight with primary antibodies diluted in blocking solution, followed by three washes in PBS and incubation with secondary antibody solution for 1 hour at RT. After three additional washes in PBS, sections were processed for hematoxylin and eosin staining, which was performed without heat using the Epredia Gemini AS Automated Slide Stainer, and lastly mounted. For RNAscope/IHC protocol, 4-μm-thick sections were processed using the RNAscope Multiplex Fluorescent Detection Kit (ACDBio), following the manufacturer′s directions. Last, stained slides were mounted with a fluorescence mounting medium (Dako).

Generation of DAAM1 and PiggyBac RNF43 expression vectors

Human *DAAM1* cDNA was purchased from TransOMIC. F.L. or truncated *DAAM1* constructs were PCR-amplified using Phusion High-Fidelity Polymerase (NEB) and cloned into pCDNA4/TO or pCS2 expression vectors, containing a Myc Tag for C-terminal fusion. To generate pBhCMV-hRNF43-IRES-mCherry and pPB-CAG-rtTA_Hyg, cDNAs of human RNF43 and hygromycin resistance were PCR-amplified as mentioned above and cloned into PiggyBac-based vectors containing tet-responsive elements, using the In-Fusion HD Cloning Kit (Clontech), according to the manufacturer′s instructions. RNF43 and reverse tetracycline responsive transcriptional activator (rtTA) expression constructs were electroporated into small intestinal (SI) organoids as described above, always in combination with the Super PiggyBac Transposase expression vector in a 2:2:1 ratio. All constructs reported here were sequence-verified using Sanger sequencing.

Cell culture, DNA transfection, and growth factor stimulation

HEK293T cells were maintained in DMEM supplemented with 10% FBS, 1% glutamine, and 1% penicillin-streptomycin, kept in a 37°C and 5% CO_2 incubator, and passaged every 5 to 7 days. Transfection was performed by using polyethylene imine (PEI; 1 μg/ml), pH 7.4, and plasmid DNA at a 5:1 ratio (*53*). Plasmid DNA used was 5 μg per 6-cm culture dish (ubiquitination and Fzd degradation assays) or 10 μg per 10-cm dish (co-IP experiments). For Fzd degradation and ubiquitination analysis, RNF43 was transfected at a ratio of 1:5 to total plasmid DNA. For Wnt3a treatment (as shown in Fig. 5, C and D), HEK293T cells were plated on 12-well plates, and upon reaching 80%, confluency cells were treated with Wnt3a CM overnight for real-time quantitative PCR or for the time indicated in the case of active β-catenin immunoblot. For the experiment shown in fig. S5A, endogenous Wnt ligand secretion was inhibited by overnight treatment with 1 μM LGK-974 (PeproTech). Subsequently, the noncanonical Wnt pathway was activated by adding rWnt5A (R&D Systems) to the culture medium at 40 or 80 ng/ml final concentration, with or without recombinant human R-spondin1 (50 ng/ml; PeproTech). For Wnt5a-induced actin cytoskeleton

rearrangements, untransfected HEK293T cells or cells transfected 48 hours earlier with pEGFP-C1 LifeAct-EGFP (Addgene, plasmid #58470) were treated with Wnt5a CM or protein (200 ng/ml) for 2 hours at 37°C, before fixation and immunostaining. Wnt5a CM was produced from commercially available L cells [American Type Culture Collection (ATCC), CRL-2814], while Wnt3a CM was produced from L cells provided by H. Clevers (Hubrecht Institute, Utrecht, Netherlands), following standard protocols. WT L cells (ATCC, CRL-2648) were instead used to produce control CM.

HEK293T Daam1/2 DKO clone generation

To generate Daam1/2 DKO clones, CRISPR-Cas9–mediated KO was performed as follows. WT HEK293T cells were seeded 3 days before transfection and a concatemer construct harboring Daam1 and Daam2 sgRNAs and Cas9-expressing vector were cotransfected, together with GFP. Successfully transfected HEK293T cells were sorted by FACS and seeded as single cells to confirm the genotype of Daam1 and Daam2 by Sanger sequencing followed by tracking of indels by decomposition (TIDE) analysis for the quantitative assessment of CRISPR gene editing. DNA oligos and primers used are listed in table S2.

Immunofluorescence and confocal imaging

Whole-mount immunostaining on organoids was performed following the protocol described by van Ineveld *et al.* (*54*), with no modifications. For HEK293T immunofluorescence, cells were grown on 12-well plates containing glass coverslips, precoated with a solution containing 0.01% poly-L-ornithine (Millipore) overnight at 37°C. Cells were then transfected and/or stimulated as described above, followed by two washes with PBS, fixation in 4% (w/v) paraformaldehyde (PFA) in PBS for 20 min, and then permeabilization with 0.2% (v/v) Triton X-100 in PBS. Coverslips were then washed with PBS, blocked for 1 hour in blocking buffer consisting of 3% (w/v) BSA in PBS at RT, and incubated with primary antibodies in blocking buffer overnight at 4°C. The next day, cells were washed three times with PBS, incubated with secondary antibodies diluted in blocking buffer for 1 hour at RT, and mounted onto glass slides with ProLong Gold antifade reagent with 4′,6-diamidino-2-phenylindole (Life Technologies) to stain cell nuclei. Cells and organoids were imaged using an inverted LSM 880 Airyscan confocal microscope (Carl Zeiss, Jena, Germany) using 405-, 488-, and 561-nm lasers for excitation, and a 20× objective (Plan Apochromat ×20/0.8). *Z*-Stacks were acquired with a resolution of 1024 pixels and snaps with a resolution of 2048 (frame size, 2048 × 2048). For scanning, the following parameters were used: unidirectional scanning, averaging number 8, 8-bit depth. Images were acquired with multitracking for each fluorophore and Zeiss ZEN Black Edition software. ZEN Blue Edition software was used for image analysis. The list of antibodies and fluorophores used for immunostaining throughout this paper is provided in table S3.

Surface Fzd5 internalization assay

SNAP-tagged Frizzled5 (SNAP-Fzd5) subcellular localization was monitored in WT and Daam1/2 KO HEK293T cells in the presence and absence of RNF43 coexpression, as previously described (*4*). SNAP-surface Alexa 549 (NEB) was applied to label surface SNAP-Fzd5 for 15 min at RT in the dark, following the manufacturer's instructions. Then, Fzd5-labelled cells were either immediately fixed (0 min) or chased for 30 min, before being fixed and processed for confocal imaging as described above. Total levels and surface fractions of SNAP-Fzd5 per cell were quantified using ImageJ. The surface levels per cell were determined by subtracting the intracellular fluorescent signal from the total SNAP-Fzd5 signal.

Nano-Glo HiBiT extracellular detection assay

A HiBiT tag was introduced to the N terminus of V5-Fzd5, after the signal peptide, so that the tag would be exposed to the extracellular side. HEK293T cells were transiently transfected with HiBiT Fzd5, with or without RNF43 (Fzd:RNF43 ratio 2:1), and plated 24 hours later onto 96-well flat clear bottom white polystyrene tissue culture–treated microplates, at 100,000 cells per well, and cultured in complete DMEM medium as described above. After an additional 24 hours, cells were washed once with PBS, and then 100 μl of fresh media were added to each well. The Nano-Glo 2x detection reagent was prepared by diluting the LgBiT protein and its furimazine substrate at 1:100 and 1:50 ratios, respectively, into the detection buffer supplied in the kit. Hence, 100 μl of detection reagent was added to the cells cultured in 100 μl of fresh media, for a 1:1 final dilution. Cells were then incubated for 10 min at RT with gentle shaking, before luciferase detection using a Synergy 2 microplate reader (Biotek). Fzd5 cell surface retention (expressed as %) was calculated using the relative light unit (RLU) readings based on the following equation: $\text{percentage retention} = \frac{\text{Fzd5;Rnf43 RLU}}{\text{Fzd5 RLU}} \times 100\%$. Background luminescence was subtracted from all samples using mock-transfected cells as controls. The assay was performed in biological triplicates.

Cell surface biotin labeling

Cell surface biotinylation was performed as previously described (*32*). Briefly, HEK293T cells were grown on six-well plates previously coated overnight with a solution (0.1 mg/ml) of poly-L-ornithine (Millipore), an important requirement to prevent cell detachment. Forty-eight hours after transfection with the DNA constructs indicated in Fig. 3A, cells were transferred on ice and washed twice with ice-cold PBS. Cell surface proteins were then biotinylated by incubation with the cell membrane-impermeable reagent EZ-Link Sulfo-NHS-SS-Biotin (1 mg/ml; Thermo Fisher Scientific) dissolved in PBS for 30 min at 4°C with gentle agitation. Cells were washed three times with ice-cold quenching solution [50 mM glycine in PBS (pH 7.4)] and twice with ice-cold PBS. Cells were kept on ice for the entire length of the labeling protocol. After the final wash, cells were lysed directly on the plates with 300 μl of TNE lysis buffer [tris-NaCl-EDTA, 50 mM tris-HCl (pH 7.4), 150 mM NaCl, 1 mM EDTA, and 1% NP-40] supplemented with protease inhibitors (Roche). Cell lysates were spun at 13,000 rpm at 4°C on a table-top centrifuge to remove cell debris, and then incubated with streptavidin agarose magnetic beads (Thermo Fisher Scientific) for 3 hours at 4°C using a head-over-head rotator to bind biotinylated proteins. An aliquot of the original cell lysate was saved for input control. At the end of the pull-down, beads were extensively washed with TNE buffer at 4°C with rotation, and then heated to 95°C in the presence of 2× Laemmli buffer (Bio-Rad) to elute proteins, followed by SDS–polyacrylamide gel electrophoresis (SDS-PAGE)/Western blot analysis. To assess pull-down specificity, a no-biotin control sample was included, and endogenous transferrin receptor was monitored as a negative control.

Mass spectrometry

To identify potential RNF43 interactors, we performed RNF43-2xFlag-2xHA IP followed by MS analysis (IP/MS) of the immunocomplexes. A total of five independent experiments were included in this assay, and RNF43 deletion constructs were used to assess interaction specificity (see below). Purification of RNF43 interactors was performed with the following four different constructs: (i) empty vector as a control for background contaminants/nonspecific protein binding, (ii) F.L. RNF43 protein (RNF43 F.L.), (iii) a truncated version of RNF43 harboring only the protease associated and transmembrane (PA-TM) domain (RNF43 Δ1), and (iv) a different truncated version of RNF43 harboring only the PA-TM-RING domain (RNF43 Δ3). The different RNF43 deletion constructs had to be used for technical reasons since an unexpected cleavage of the F.L. protein was found to occur during sample processing before MS analysis, yielding only the intracellular domain of the original F.L. RNF43. To overcome this and avoid possible artifacts due to protein mislocalization, a complementary deletion form containing the extracellular and transmembrane domains was generated (RNF43 Δ1) and used to repeat the analysis. We noticed that the removal of the C terminus (amino acids 524 to 784) from the F.L. protein greatly increased its stability (RNF43 Δ3), and therefore, the experiment included this form as well. HEK293T cells were transfected with pcDNA3-RNF43-2xFlag-2xHA (F.L., Δ1 or Δ3). Cells were harvested and subsequently lysed in lysis buffer [50 mM tris-HCl (pH 7.5), 150 mM NaCl, 1 mM EDTA, and 0.5% NP-40 plus protease and phosphatase inhibitors]. RNF43 was immunopurified with anti-FLAG agarose resin (Sigma-Aldrich). The beads were washed, and proteins were eluted by competition with FLAG peptide (Sigma-Aldrich). The eluate was then subjected to a second immunopurification with anti-hemagglutinin (HA) resin (12CA5 monoclonal antibody cross-linked to protein G–Sepharose; Invitrogen) before elution in Laemmli sample buffer. The final eluate was separated by SDS-PAGE and proteins were visualized by Coomassie colloidal blue staining. Bands were sliced out carefully from the gels with a scalpel and subjected to in-gel trypsin (Promega) digestion. Gel pieces were then reduced, alkylated, and digested according to a published protocol (*55*). For mass spectrometric analysis, peptides recovered from in-gel digestion were separated with a C18 column and introduced by nano-electrospray into an LTQ Orbitrap spectrometer (Thermo Fisher Scientific). Peak lists were generated from the MS/MS spectra with MaxQuant, and then searched against the SwissProt human database with the Mascot search engine (Matrix Science). Carbaminomethylation (+57 Da) was set as a fixed modification and protein N-terminal acetylation and methionine oxidation as variable modifications. Peptide tolerance was set to 20 parts per million (ppm) and fragment ion tolerance was set to 0.5 Da, allowing two missed cleavages with trypsin enzyme. The hit list containing all identified peptides and their relative abundance is provided in table S1.

CRISPR-Cas9 organoid screening

To achieve multiple gene KO using CRISPR-Cas9 technology, we used a protocol established by our laboratory (*15*, *16*). For the planned screening, we generated constructs containing three or four different gRNAs, depending on the number of paralogues for each candidate: for genes with only one paralogue, we designed two gRNAs to target each gene and cloned these into our 4 gRNA-concatemer vector (*15*, *16*), whereas for genes with no paralogues, three different gRNAs were designed to target the same gene and thus increase the efficiency of KO. In this way, we generated gRNAs against all the selected MS hits and their paralogues. To perform the CRISPR KO screening, the gRNA-concatemer vectors were introduced together with a Cas9 expression plasmid into doxycycline-inducible RNF43 (iRNF43) organoids by electroporation, using the protocol described above. In summary, gRNA vectors were generated for the selected genes as part of a CRISPR-concatemer strategy for multiple gene KO in RNF43-overexpressing organoids. Following recovery from electroporation, iRNF43 organoids were subjected to prolonged doxycycline treatment, and their survival was monitored after several rounds of splitting to functionally screen the selected MS hits. The same number of cells was seeded into each well and all wells were split in parallel at the same ratio for each round of passaging. KO of the destruction complex component Axin was used as a positive control, as Axin KO allows organoid survival even after prolonged RNF43 overexpression, in contrast to WT iRNF43 organoids which die around passage #2 when cultured in a Dox-supplemented medium.

Immunoprecipitation

To assess RNF43 and Daam1 interaction, we performed IP assays as previously described (*56*), with some modifications. Briefly, HEK293T cells seeded onto 10-cm plates were transfected with the constructs indicated, using PEI and 10 μg of total DNA. Forty-eight hours after transfection, cells were lysed in 1 ml of IP lysis buffer [10 mM tris-HCl (pH 7.5), 100 mM NaCl, 2 mM EDTA, 1 mM EGTA, 0.5% (v/v) NP-40, and 10% (v/v) glycerol] supplemented with a protease inhibitor cocktail (cOmplete, EDTA-free, Roche). Cell lysates were clarified by centrifugation (13,000 rpm, 4°C), and then precleared with 20 μl of protein A/G PLUS agarose beads (Santa Cruz Biotechnology, sc-2003) for 1 hour at 4°C, on a head-over-head rotator. Beads were removed by centrifugation and cleared lysates were then incubated with 2 μg of primary antibody (anti-HA, Thermo Fisher Scientific) overnight at 4°C on a head-over-head rotator. Supernatants were then incubated with 40 μl of protein A/G agarose beads for 2 hours at 4°C on rotation, extensively washed in lysis buffer, resuspended in 40 μl of SDS 2x Laemmli buffer (Bio-Rad), and heated for 5 min at 95°C to elute immunocomplexes, followed by analysis through SDS-PAGE and Western blot. For the experiment shown in fig. S3 (B and C), IP was conducted with anti-Flag (Sigma-Aldrich, M8823) or anti-V5 magnetic beads (ChromoTek V5-Trap, v5tma), respectively, following the manufacturer′s protocol.

Ubiquitination assay

HEK293T cells seeded in 6-cm plates and maintained in DMEM with 10% FBS and penicillin-streptomycin were transfected with ubiquitin-Myc-6xHis, V5-Frizzled5, and RNF43-2xFlag-2xHA using PEI. Where required, transfected cells were incubated with 10 nM bafilomycin A1 (BafA1) overnight before lysis. Two days after transfection, samples were harvested and lysed with 500 μl of IP lysis buffer (as described above) supplemented with a protease inhibitor cocktail (cOmplete, EDTA-free, Roche) and 10 mM *N*-ethylmaleimide (Sigma-Aldrich, E3876). Lysates were then incubated with V5-Trap magnetic agarose beads (ChromoTek) overnight at 4°C before being processed for Western blot analysis.

Wnt5a-induced active Rho assay

Active Rho pull-down was performed as previously described (*57*), with some modifications. HEK293T cells were stimulated with rWnt5a at a concentration of 200 or 400 ng/ml for 30 min at 37°C. Next, cells were quickly washed with ice-cold PBS and lysed in ice-cold lysis buffer [25 mM Tris-HCl (pH 7.2), 150 mM NaCl, 5 mM $MgCl_2$, 1% NP-40, and 5% glycerol]. Crude lysates were then clarified by centrifugation and the supernatant was incubated with glutathione magnetic beads (Thermo Fisher Scientific), conjugated with the Rhotekin Rho-binding domain–GST fusion protein (produced from Addgene, plasmid #15247), for 1 hour at 4°C, before proceeding to Western blot analysis.

Western blotting

SDS-PAGE and Western blots were performed using precast gradient gels (Thermo Fisher Scientific), using standard protocols. Blotted nitrocellulose membranes were analyzed using the Li-Cor software Odyssey 3.0. All primary and secondary antibodies were diluted either in tris-buffered saline plus 0.1% Tween 20 (TBST) containing 2.5% (w/v) of Blotting-Grade Blocker (Bio-Rad), or in Li-Cor Intercept (TBS) blocking buffer supplemented with 0.1% Tween 20. The list of antibodies used and their dilution is provided in table S4.

Xenopus husbandry and embryo injection

WT frogs were obtained from the European *Xenopus* Resource Center, UK, and NASCO, USA, and group-housed at the Institute of Molecular Pathology facilities. All animal handling and surgical procedures were carried out adhering to the guidelines of the Austrian Animal Care and Use Committee. In vitro fertilization was performed as previously described (*58*). Briefly, testes were surgically removed from a male frog anesthetized in 0.03% tricaine methanesulfonate (Sigma-Aldrich, MS222), and a sperm suspension was obtained by crushing each testis in 1 ml of 1× Marc′s modified Ringers [MMR, 0.1 M NaCl, 2.0 mM KCl, 1 mM MgSO4, 2 mM CaCl2, and 5 mM Hepes (pH 7.4)]. Ovulation of female frogs was induced the night before the experiment by injecting 500 IU of human chorionic gonadotropin. On the day of the experiment, frogs were allowed to spontaneously lay eggs in a high-salt solution (1.2× MMR). Laid eggs were collected and fertilized with 200 to 300 μl of sperm suspension. To remove the jelly coat, fertilized eggs were treated with 2% cysteine in 0.1× MMR, pH 7.8, for about 7 min at RT. Dejellied embryos were then cultured in 0.1× MMR′s solution and staged according to Nieuwkoop and Faber (*59*). Translation-inhibiting MO antisense oligos specific for *Xenopus daam1* and *daam2* were obtained from GeneTools. The *daam1* MO sequence was previously reported (*60*), while *daam2* MO was designed ex novo for this study. *Xenopus* genomic sequence deposited at Xenbase was used to verify that the designed *daam* MOs target both L and S homeologs (*61*). All MO sequences used in this study are listed in table S2. For embryo injections, 30 ng total/embryo of *daam1/2* MOs were injected alone or in combination into the two dorsal blastomeres of four-cell stage embryos. Standard MO (CoMO; targeting a human beta-globin intron mutation that causes beta-thalassemia) was used as a negative control and injected at a similar concentration. For *wnt8* injection, 32 ng total/embryo of *pCSKA-xwnt8* (Addgene, #16866) plasmid DNA was injected into the two dorsal blastomeres of four-cell stage embryos. After injection, embryos were collected at the early tailbud stage, fixed in 4% PFA in PBS for 2 hours at RT, and washed extensively with PBS to remove residual PFA. Images were acquired on a color camera–equipped stereomicroscope (Zeiss). To assess MO specificity, we cloned the 5′ coding or untranslated region of *Xenopus daam1* and *daam2* genes, respectively, containing the MO binding sites, upstream of the *gfp* open reading frame, into the $pCS2^+$ vector. The presence of *daam* sequences did not affect GFP fluorescence. Plasmids were then linearized using NotI restriction enzyme and mRNA was transcribed in vitro using mMESSAGE mMACHINE SP6 Transcription Kit (Thermo Fisher Scientific), following the manufacturer′s instructions. A total (250 pg) of *d1/2-gfp* mRNAs were injected animally into two blastomeres of four- or eight-cell stage embryos, together with 30 ng total of *daam1/2* or control MOs (as indicated in fig. S6). Last, injected embryos were collected at the neurula stage and processed for Western blot analysis.

RT-qPCR

RNA extraction from HEK293T cells and mouse small intestinal organoids, cDNA preparation, and RT-qPCR were performed according to established protocols (*62*), with minor modifications. Briefly, HEK293T cells from single wells of a six-well plate were pelleted and total RNA was extracted using the RNeasy MiniKit (QIAGEN), following the manufacturer′s instructions. For organoid total RNA preparation, three single wells of a 48-well plate were pooled together after removing Matrigel with Cell Recovery Solution (Corning), for 1 hour at 4°C. One microgram of total RNA was used for cDNA synthesis with $Oligo(dT)_{18–22}$ primers by SuperScript III Reverse Transcriptase (Thermo Fisher Scientific). Two microliters of cDNA was then used for qRT-PCR, which was performed on a CFX Connect Real-Time System thermal cycler (Bio-Rad), using GoTaq qPCR master mix (Promega) and including two to three biological replicates for each marker and reference gene. Expression levels were normalized to housekeeping gene actin. Primer sequences are listed in table S2.

Statistics

Statistical analysis was performed using the corresponding functions in Microsoft Excel as well as using R software. Student′s unpaired *t* tests (two-tailed) were used to compare differences between the two groups. Data from three or more independent groups were analyzed using a two-way analysis of variance (ANOVA). For all statistic tests, $^*P < 0.05$, $^{**}P < 0.01$, or $^{***}P < 0.001$ were considered as thresholds for statistical significance. Unless indicated otherwise in the figure legends, all data presented are mean values ± SD.

Supplementary Materials

This PDF file includes:

Figs. S1 to S9
Legend for table S1
Tables S2 to S4

Other Supplementary Material for this manuscript includes the following:

Table S1

REFERENCES AND NOTES

1. J. Beumer, H. Clevers, Cell fate specification and differentiation in the adult mammalian intestine. *Nat. Rev. Mol. Cell Biol.* **22**, 39–53 (2021).

2. G. Colozza, S. Y. Park, B. K. Koo, Clone wars: From molecules to cell competition in intestinal stem cell homeostasis and disease. *Exp. Mol. Med.* **54**, 1367–1378 (2022).
3. R. Nusse, H. Clevers, Wnt/β-catenin signaling, disease, and emerging therapeutic modalities. *Cell* **169**, 985–999 (2017).
4. B. K. Koo, M. Spit, I. Jordens, T. Y. Low, D. E. Stange, M. van de Wetering, J. H. van Es, S. Mohammed, A. J. Heck, M. M. Maurice, H. Clevers, Tumour suppressor RNF43 is a stem-cell E3 ligase that induces endocytosis of Wnt receptors. *Nature* **488**, 665–669 (2012).
5. H. X. Hao, Y. Xie, Y. Zhang, O. Charlat, E. Oster, M. Avello, H. Lei, C. Mickanin, D. Liu, H. Ruffner, X. Mao, Q. Ma, R. Zamponi, T. Bouwmeester, P. M. Finan, M. W. Kirschner, J. A. Porter, F. C. Serluca, F. Cong, ZNRF3 promotes Wnt receptor turnover in an R-spondin-sensitive manner. *Nature* **485**, 195–200 (2012).
6. H. F. Farin, I. Jordens, M. H. Mosa, O. Basak, J. Korving, D. V. Tauriello, K. de Punder, S. Angers, P. J. Peters, M. M. Maurice, H. Clevers, Visualization of a short-range Wnt gradient in the intestinal stem-cell niche. *Nature* **530**, 340–343 (2016).
7. W. de Lau, N. Barker, T. Y. Low, B. K. Koo, V. S. Li, H. Teunissen, P. Kujala, A. Haegebarth, P. J. Peters, M. van de Wetering, D. E. Stange, J. E. van Es, D. Guardavaccaro, R. B. Schasfoort, Y. Mohri, K. Nishimori, S. Mohammed, A. J. Heck, H. Clevers, Lgr5 homologues associate with Wnt receptors and mediate R-spondin signalling. *Nature* **476**, 293–297 (2011).
8. A. Glinka, C. Dolde, N. Kirsch, Y. L. Huang, O. Kazanskaya, D. Ingelfinger, M. Boutros, C. M. Cruciat, C. Niehrs, LGR4 and LGR5 are R-spondin receptors mediating Wnt/β-catenin and Wnt/PCP signalling. *EMBO Rep.* **12**, 1055–1061 (2011).
9. T. Tsukiyama, J. Zou, J. Kim, S. Ogamino, Y. Shino, T. Masuda, A. Merenda, M. Matsumoto, Y. Fujioka, T. Hirose, S. Terai, H. Takahashi, T. Ishitani, K. I. Nakayama, Y. Ohba, B. K. Koo, S. Hatakeyama, A phospho-switch controls RNF43-mediated degradation of Wnt receptors to suppress tumorigenesis. *Nat. Commun.* **11**, 4586 (2020).
10. N. Giebel, A. de Jaime-Soguero, A. G. del Arco, J. J. M. Landry, M. Tietje, L. Villacorta, V. Benes, V. Fernandez-Saiz, S. P. Acebron, USP42 protects ZNRF3/RNF43 from R-spondin-dependent clearance and inhibits Wnt signalling. *EMBO Rep.* **22**, e51415 (2021).
11. G. Colozza, B. K. Koo, Ub and Dub of RNF43/ZNRF3 in the WNT signalling pathway. *EMBO Rep.* **22**, e52970 (2021).
12. T. Sato, J. H. van Es, H. J. Snippert, D. E. Stange, R. G. Vries, M. van den Born, N. Barker, N. F. Shroyer, M. van de Wetering, H. Clevers, Paneth cells constitute the niche for Lgr5 stem cells in intestinal crypts. *Nature* **469**, 415–418 (2011).
13. H. C. Clevers, C. L. Bevins, Paneth cells: Maestros of the small intestinal crypts. *Annu. Rev. Physiol.* **75**, 289–311 (2013).
14. S. Kuhn, M. Geyer, Formins as effector proteins of Rho GTPases. *Small GTPases* **5**, e29513 (2014).
15. A. Andersson-Rolf, A. Merenda, R. C. Mustata, T. Li, S. Dietmann, B. K. Koo, Simultaneous paralogue knockout using a CRISPR-concatemer in mouse small intestinal organoids. *Dev. Biol.* **420**, 271–277 (2016).
16. A. Merenda, A. Andersson-Rolf, R. C. Mustata, T. Li, H. Kim, B. K. Koo, A protocol for multiple gene knockout in mouse small intestinal organoids using a CRISPR-concatemer. *J. Vis. Exp.* **125**, e55916 (2017).
17. T. Radaszkiewicz, M. Noskova, K. Gomoryova, O. Vondalova Blanarova, K. A. Radaszkiewicz, M. Pickova, R. Vichova, T. Gybel, K. Kaiser, L. Demkova, L. Kucerova, T. Barta, D. Potesil, Z. Zdrahal, K. Soucek, V. Bryja, RNF43 inhibits WNT5A-driven signaling and suppresses melanoma invasion and resistance to the targeted therapy. *eLife* **10**, (2021).
18. R. Habas, Y. Kato, X. He, Wnt/Frizzled activation of Rho regulates vertebrate gastrulation and requires a novel formin homology protein Daam1. *Cell* **107**, 843–854 (2001).
19. W. Liu, A. Sato, D. Khadka, R. Bharti, H. Diaz, L. W. Runnels, R. Habas, Mechanism of activation of the formin protein Daam1. *Proc. Natl. Acad. Sci. U.S.A.* **105**, 210–215 (2008).
20. A. Gurney, F. Axelrod, C. J. Bond, J. Cain, C. Chartier, L. Donigan, M. Fischer, A. Chaudhari, M. Ji, A. M. Kapoun, A. Lam, S. Lazetic, S. Ma, S. Mitra, I. K. Park, K. Pickell, A. Sato, S. Satyal, M. Stroud, H. Tran, W. C. Yen, J. Lewicki, T. Hoey, Wnt pathway inhibition via the targeting of Frizzled receptors results in decreased growth and tumorigenicity of human tumors. *Proc. Natl. Acad. Sci. U.S.A.* **109**, 11717–11722 (2012).
21. M. K. Schwinn, T. Machleidt, K. Zimmerman, C. T. Eggers, A. S. Dixon, R. Hurst, M. P. Hall, L. P. Encell, B. F. Binkowski, K. V. Wood, CRISPR-mediated tagging of endogenous proteins with a luminescent peptide. *ACS Chem. Biol.* **13**, 467–474 (2018).
22. M. E. Boursier, S. Levin, K. Zimmerman, T. Machleidt, R. Hurst, B. L. Butler, C. T. Eggers, T. A. Kirkland, K. V. Wood, R. Friedman Ohana, The luminescent HiBiT peptide enables selective quantitation of G protein-coupled receptor ligand engagement and internalization in living cells. *J. Biol. Chem.* **295**, 5124–5135 (2020).
23. H. Marei, W. K. Tsai, Y. S. Kee, K. Ruiz, J. He, C. Cox, T. Sun, S. Penikalapati, P. Dwivedi, M. Choi, D. Kan, P. Saenz-Lopez, K. Dorighi, P. Zhang, Y. T. Kschonsak, N. Kljavin, D. Amin, I. Kim, A. G. Mancini, T. Nguyen, C. Wang, E. Janezic, A. Doan, E. Mai, H. Xi, C. Gu, M. Heinlein, B. Biehs, J. Wu, I. Lehoux, S. Harris, L. Comps-Agrar, D. Seshasayee, F. J. de Sauvage, M. Grimmer, J. Li, N. J. Agard, E. M. F. de Sousa, Antibody targeting of E3 ubiquitin ligases for receptor degradation. *Nature* **610**, 182–189 (2022).
24. X. Jiang, O. Charlat, R. Zamponi, Y. Yang, F. Cong, Dishevelled promotes Wnt receptor degradation through recruitment of ZNRF3/RNF43 E3 ubiquitin ligases. *Mol. Cell* **58**, 522–533 (2015).
25. A. Bottcher, M. Buttner, S. Tritschler, M. Sterr, A. Aliluev, L. Oppenlander, I. Burtscher, S. Sass, M. Irmler, J. Beckers, C. Ziegenhain, W. Enard, A. C. Schamberger, F. M. Verhamme, O. Eickelberg, F. J. Theis, H. Lickert, Non-canonical Wnt/PCP signalling regulates intestinal stem cell lineage priming towards enteroendocrine and Paneth cell fates. *Nat. Cell Biol.* **23**, 23–31 (2021).
26. R. Wadsworth, "The role of SRGAP2 in vertebrate gastrulation," thesis, Temple University (2016).
27. M. Nishita, S. K. Yoo, A. Nomachi, S. Kani, N. Sougawa, Y. Ohta, S. Takada, A. Kikuchi, Y. Minami, Filopodia formation mediated by receptor tyrosine kinase Ror2 is required for Wnt5a-induced cell migration. *J. Cell Biol.* **175**, 555–562 (2006).
28. R. Jaiswal, D. Breitsprecher, A. Collins, I. R. Correa Jr., M. Q. Xu, B. L. Goode, The formin Daam1 and fascin directly collaborate to promote filopodia formation. *Curr. Biol.* **23**, 1373–1379 (2013).
29. W. Luo, Z. Z. Lieu, E. Manser, A. D. Bershadsky, M. P. Sheetz, Formin DAAM1 organizes actin filaments in the cytoplasmic nodal actin network. *PLOS ONE* **11**, e0163915 (2016).
30. C. Niehrs, The role of Xenopus developmental biology in unraveling Wnt signalling and antero-posterior axis formation. *Dev. Biol.* **482**, 1–6 (2022).
31. A. Glinka, W. Wu, H. Delius, A. P. Monaghan, C. Blumenstock, C. Niehrs, Dickkopf-1 is a member of a new family of secreted proteins and functions in head induction. *Nature* **391**, 357–362 (1998).
32. Y. Ding, G. Colozza, E. A. Sosa, Y. Moriyama, S. Rundle, L. Salwinski, E. M. De Robertis, *Bighead is a Wnt antagonist secreted by the Xenopus* Spemann organizer that promotes Lrp6 endocytosis. *Proc. Natl. Acad. Sci. U.S.A.* **115**, E9135–E9144 (2018).
33. G. Colozza, Y. Jami-Alahmadi, A. Dsouza, N. Tejeda-Munoz, L. V. Albrecht, E. A. Sosa, J. A. Wohlschlegel, E. M. De Robertis, Wnt-inducible Lrp6-APEX2 interacting proteins identify ESCRT machinery and Trk-fused gene as components of the Wnt signaling pathway. *Sci. Rep.* **10**, 21555 (2020).
34. P. Janovska, V. Bryja, Wnt signalling pathways in chronic lymphocytic leukaemia and B-cell lymphomas. *Br. J. Pharmacol.* **174**, 4701–4715 (2017).
35. P. Janovska, E. Normant, H. Miskin, V. Bryja, Targeting casein kinase 1 (CK1) in hematological cancers. *Int. J. Mol. Sci.* **21**, (2020).
36. E. Bader, A. Migliorini, M. Gegg, N. Moruzzi, J. Gerdes, S. S. Roscioni, M. Bakhti, E. Brandl, M. Irmler, J. Beckers, M. Aichler, A. Feuchtinger, C. Leitzinger, H. Zischka, R. Wang-Sattler, M. Jastroch, M. Tschop, F. Machicao, H. Staiger, H. U. Haring, H. Chmelova, J. A. Chouinard, N. Oskolkov, O. Korsgren, S. Speier, H. Lickert, Identification of proliferative and mature β-cells in the islets of Langerhans. *Nature* **535**, 430–434 (2016).
37. B. K. Koo, J. H. van Es, M. van den Born, H. Clevers, Porcupine inhibitor suppresses paracrine Wnt-driven growth of Rnf43;Znrf3-mutant neoplasia. *Proc. Natl. Acad. Sci. U.S.A.* **112**, 7548–7550 (2015).
38. Y. S. Kida, T. Sato, K. Y. Miyasaka, A. Suto, T. Ogura, Daam1 regulates the endocytosis of EphB during the convergent extension of the zebrafish notochord. *Proc. Natl. Acad. Sci. U.S.A.* **104**, 6708–6713 (2007).
39. G. H. Kim, J. K. Han, Essential role for beta-arrestin 2 in the regulation of *Xenopus* convergent extension movements. *EMBO J.* **26**, 2513–2526 (2007).
40. G. Colozza, B. K. Koo, Wnt/β-catenin signaling: Structure, assembly and endocytosis of the signalosome. *Dev. Growth Differ.* **63**, 199–218 (2021).
41. L. V. Albrecht, N. Tejeda-Munoz, E. M. De Robertis, Cell biology of canonical wnt signaling. *Annu. Rev. Cell Dev. Biol.* **37**, 369–389 (2021).
42. G. Lian, M. Dettenhofer, J. Lu, M. Downing, A. Chenn, T. Wong, V. Sheen, Filamin A- and formin 2-dependent endocytosis regulates proliferation via the canonical Wnt pathway. *Development* **143**, 4509–4520 (2016).
43. W. de Lau, W. C. Peng, P. Gros, H. Clevers, The R-spondin/Lgr5/Rnf43 module: Regulator of Wnt signal strength. *Genes Dev.* **28**, 305–316 (2014).
44. H. X. Hao, X. Jiang, F. Cong, Control of Wnt receptor turnover by R-spondin-ZNRF3/RNF43 signaling module and its dysregulation in cancer. *Cancers* **8**, (2016).
45. F. Farnhammer, G. Colozza, J. Kim, RNF43 and ZNRF3 in Wnt signaling - a master regulator at the membrane. *J. Stem Cells*, (2023).
46. G. X. Zheng, J. M. Terry, P. Belgrader, P. Ryvkin, Z. W. Bent, R. Wilson, S. B. Ziraldo, T. D. Wheeler, G. P. McDermott, J. Zhu, M. T. Gregory, J. Shuga, L. Montesclaros, J. G. Underwood, D. A. Masquelier, S. Y. Nishimura, M. Schnall-Levin, P. W. Wyatt, C. M. Hindson, R. Bharadwaj, A. Wong, K. D. Ness, L. W. Beppu, H. J. Deeg, C. McFarland, K. R. Loeb, W. J. Valente, N. G. Ericson, E. A. Stevens, J. P. Radich, T. S. Mikkelsen, B. J. Hindson, J. H. Bielas, Massively parallel digital transcriptional profiling of single cells. *Nat. Commun.* **8**, 14049 (2017).
47. Y. Hao, S. Hao, E. Andersen-Nissen, W. M. Mauck 3rd, S. Zheng, A. Butler, M. J. Lee, A. J. Wilk, C. Darby, M. Zager, P. Hoffman, M. Stoeckius, E. Papalexi, E. P. Mimitou, J. Jain, A. Srivastava, T. Stuart, L. M. Fleming, B. Yeung, A. J. Rogers, J. M. McElrath, C. A. Blish, R. Gottardo, P.

Smibert, R. Satija, Integrated analysis of multimodal single-cell data. *Cell* **184**, 3573–3587. e29 (2021).
48. C. S. McGinnis, L. M. Murrow, Z. J. Gartner, DoubletFinder: Doublet detection in single-Cell RNA sequencing data using artificial nearest neighbors. *Cell Syst* **8**, 329–337.e4 (2019).
49. I. Korsunsky, N. Millard, J. Fan, K. Slowikowski, F. Zhang, K. Wei, Y. Baglaenko, M. Brenner, P. R. Loh, S. Raychaudhuri, Fast, sensitive and accurate integration of single-cell data with Harmony. *Nat. Methods* **16**, 1289–1296 (2019).
50. M. Fujii, M. Matano, K. Toshimitsu, A. Takano, Y. Mikami, S. Nishikori, S. Sugimoto, T. Sato, Human intestinal organoids maintain self-renewal capacity and cellular diversity in niche-inspired culture condition. *Cell Stem Cell* **23**, 787–793.e6 (2018).
51. D. G. Bunis, J. Andrews, G. K. Fragiadakis, T. D. Burt, M. Sirota, dittoSeq: Universal user-friendly single-cell and bulk RNA sequencing visualization toolkit. *Bioinformatics* **36**, 5535–5536 (2021).
52. M. I. Love, W. Huber, S. Anders, Moderated estimation of fold change and dispersion for RNA-seq data with DESeq2. *Genome Biol.* **15**, 550 (2014).
53. P. Paclikova, O. Bernatik, T. W. Radaszkiewicz, V. Bryja, The n-terminal part of the dishevelled DEP domain is required for Wnt/β-Catenin signaling in mammalian cells. *Mol. Cell. Biol.* **37**, (2017).
54. R. L. van Ineveld, H. C. R. Ariese, E. J. Wehrens, J. F. Dekkers, A. C. Rios, Single-cell resolution three-dimensional imaging of intact organoids. *J. Vis. Exp.* **160**, e60709 (2020).
55. A. Shevchenko, M. Wilm, O. Vorm, M. Mann, Mass spectrometric sequencing of proteins silver-stained polyacrylamide gels. *Anal. Chem.* **68**, 850–858 (1996).
56. Y. Ding, G. Colozza, K. Zhang, Y. Moriyama, D. Ploper, E. A. Sosa, M. D. J. Benitez, E. M. De Robertis, Genome-wide analysis of dorsal and ventral transcriptomes of the Xenopus laevis gastrula. *Dev. Biol.* **426**, 176–187 (2017).
57. X. D. Ren, W. B. Kiosses, M. A. Schwartz, Regulation of the small GTP-binding protein Rho by cell adhesion and the cytoskeleton. *EMBO J.* **18**, 578–585 (1999).
58. G. Colozza, E. M. De Robertis, Dact-4 is a Xenopus laevis Spemann organizer gene related to the Dapper/Frodo antagonist of β-catenin family of proteins. *Gene Expr. Patterns* **38**, 119153 (2020).
59. P. D. Nieuwkoop, J. Faber, *Normal Table of Xenopus laevis (Daudin)* (North-Holland Publishing Company, 1967).
60. O. Ossipova, I. Chuykin, C. W. Chu, S. Y. Sokol, Vangl2 cooperates with Rab11 and Myosin V to regulate apical constriction during vertebrate gastrulation. *Development* **142**, 99–107 (2015).
61. A. M. Session, Y. Uno, T. Kwon, J. A. Chapman, A. Toyoda, S. Takahashi, A. Fukui, A. Hikosaka, A. Suzuki, M. Kondo, S. J. van Heeringen, I. Quigley, S. Heinz, H. Ogino, H. Ochi, U. Hellsten, J. B. Lyons, O. Simakov, N. Putnam, J. Stites, Y. Kuroki, T. Tanaka, T. Michiue, M. Watanabe, O. Bogdanovic, R. Lister, G. Georgiou, S. S. Paranjpe, I. van Kruijsbergen, S. Shu, J. Carlson, T. Kinoshita, Y. Ohta, S. Mawaribuchi, J. Jenkins, J. Grimwood, J. Schmutz, T. Mitros, S. V. Mozaffari, Y. Suzuki, Y. Haramoto, T. S. Yamamoto, C. Takagi, R. Heald, K. Miller, C. Haudenschild, J. Kitzman, T. Nakayama, Y. Izutsu, J. Robert, J. Fortriede, K. Burns, V. Lotay, K. Karimi, Y. Yasuoka, D. S. Dichmann, M. F. Flajnik, D. W. Houston, J. Shendure, L. DuPasquier, P. D. Vize, A. M. Zorn, M. Ito, E. M. Marcotte, J. B. Wallingford, Y. Ito, M. Asashima, N. Ueno, Y. Matsuda, G. J. Veenstra, A. Fujiyama, R. M. Harland, M. Taira, D. S. Rokhsar, Genome evolution in the allotetraploid frog *Xenopus laevis*. *Nature* **538**, 336–343 (2016).
62. G. Colozza, E. M. De Robertis, Maternal syntabulin is required for dorsal axis formation and is a germ plasm component in *Xenopus*. *Differentiation* **88**, 17–26 (2014).

Acknowledgments: We thank members of the Koo, Elling, and Urban laboratories for valuable discussions and critical comments; R. Zietlow for reading and editing the manuscript; VBC core facilities (especially the Histology Facility, which performed RNAscope staining, BioOptics, Molecular Biology, and the animal caretakers), and the laboratory of E. Tanaka for providing the frog embryos. Single-cell RNA-seq was performed by the Next Generation Sequencing Facility at Vienna BioCenter Core Facilities (VBCF). This work is dedicated to the memory of Maurizio Colozza (1950–2021) and Bong Lee (1959–2023). **Funding:** Work in the Koo laboratory is supported by core funding from the Institute of Molecular Biotechnology (IMBA) of the Austrian Academy of Sciences; ERC starting grant, Troy Stem cells, 639050; and the Institute for Basic Science (IBS). G.C. is supported by the Austrian Science Fund (FWF), Lise Meitner Program M 2976. S.-H.S.W. is supported by the DOC Fellowship of the Austrian Academy of Sciences. Research in the V.B. laboratory is funded by the Czech Science Foundation (GX19-28347X) and by the project National Institute for Cancer Research (Program EXCELES, ID Project No. LX22NPO5102) (funded by the European Union Next GenerationEU). M.M.M. is funded by Oncode Institute, which is partly financed by the Dutch Cancer Society, the Dutch Cancer Society KWF Grant 13112, Zon-MW TOP grant 91218050, and the NWO Gravitation project IMAGINE!. **Author contributions:** Conceptualization: G.C., A.M., J.K., and B.-K.K. Methodology and data acquisition: G.C., A.M., S.-H.S.W., A.C.-B., T.W.R., I.J., J.-H.L., A.-D.B., F.F., T.Y.L., and J.K. Coordination of collaboration: T.Y.L., M.M.M., V.B., and B.-K.K. Writing: G.C., H.L., J.K., and B.-K.K. Supervision: M.M.M., V.B., and B.-K.K. **Competing interests:** The authors declare that they have no competing interests. **Data and materials availability:** All data needed to evaluate the conclusions in the paper are present in the paper and/or the Supplementary Materials. The mass spectrometry proteomics datasets associated with this study have been deposited to the JPOST repository (https://repository.jpostdb.org/) with ID nos. JPST002210 or PXD043151 and are publicly and freely accessible. The single-cell RNA-seq dataset is under GEO accession GSE239710, available at www.ncbi.nlm.nih.gov/geo/query/acc.cgi?acc=GSE239710. All unique/stable reagents generated in this study will be freely available from the lead contact to academic researchers pending a completed material transfer agreement. For inquiries, please contact koobk@ibs.re.kr (B.-K.K.).

Submitted 25 March 2023
Accepted 25 October 2023
Published 24 November 2023
10.1126/sciadv.adh9673

ScienceAdvances

Intestinal Paneth cell differentiation relies on asymmetric regulation of Wnt signaling by Daam1/2

Gabriele Colozza, Heetak Lee, Alessandra Merenda, Szu-Hsien Sam Wu, Andrea Català-Bordes, Tomasz W. Radaszkiewicz, Ingrid Jordens, Ji-Hyun Lee, Aileen-Diane Bamford, Fiona Farnhammer, Teck Yew Low, Madelon M. Maurice, Vít#zslav Bryja, Jihoon Kim, and Bon-Kyoung Koo

Sci. Adv. **9** (47), eadh9673. DOI: 10.1126/sciadv.adh9673